JPL PUBLICATION 84-50, PART II

(NASA-CR-174110) AN EXPERIMENTAL INVESTIGATION OF TWO-DIMENSIONAL THRUST AUGMENTING EJECTORS, PART 2 Final Report, Jan. 1982 - Dec. 1983 (Jet Propulsion Lab.) 96 p HC A05/MF A01 CSCL 21E G3/07

N85-12895

Unclas 24610

An Experimental Investigation of Two-Dimensional Thrust Augmenting Ejectors: Final Report, Part II

L. Bernal
V. Sarohia

August 15, 1984

Prepared for

Air Force Flight Dynamics Laboratories
Air Force Office of Scientific Research
NASA Ames Research Center
Naval Air Development Center
and

National Aeronautics and Space Administration
by

Jet Propulsion Laboratory
California Institute of Technology
Pasadena, California

JPL PUBLICATION 84-50, PART II

An Experimental Investigation of Two-Dimensional Thrust Augmenting Ejectors: Final Report, Part II

L. Bernal
V. Sarohia

August 15, 1984

Prepared for

Air Force Flight Dynamics Laboratories
Air Force Office of Scientific Research
NASA Ames Research Center
Naval Air Development Center
and
National Aeronautics and Space Administration
by

Jet Propulsion Laboratory
California Institute of Technology
Pasadena, California

The research described in this paper was carried out by the Jet Propulsion Laboratory, California Institute of Technology, and was sponsored by the U. S. Department of the Air Force, the U. S. Department of the Navy, and the National Aeronautics and Space Administration.

PREFACE

This volume is the second of two parts. Part I emphasizes the Laser Doppler Velocimetry developed especially for this program. Part II presents detailed cold flow measurements along with preliminary primary hot flow data.

ACKNOWLEDGEMENTS

This report presents the results of one phase of research carried out at the Jet Propulsion Laboratory, California Institute of Technology, Contract NAS7-918, Task Orders RD-182/Amendment 94, RD-182/Amendment 117, RD-182/Amendment 138, and RD-65/Amendment 369, jointly funded respectively by the Air Force Flight Dynamics Laboratories (AFFDL MIPR No. FY 14568000005), the Naval Air Development Center (MIPR No. N62269/80/MP/00034), the Air Force Office of Scientific Research (AFOSR-ISSA-81-00029), and the NASA-Ames Research Center (505-42-71-03-69). The authors extend their gratitude to Dr. K. Nagaraja, Dr. K. Green, Dr. J. Wilson, and Mr. D. Koenig for many technical suggestions throughout the program.

We extend our appreciation to Miss P. Logan for the analysis of the experimental data taken with the Laser Doppler Velocimeter. We are also grateful to Dr. M. Azzazy for the critical technical review of this report. The assistance of Messrs. Stan Kikkert, Barney Green, and Wayne Bixler for design, fabrication, assembly, and acquisition of the experimental data is greatly appreciated.

ABSTRACT

The flow-field within a two-dimensional thrust augmenting ejector has been documented experimentally. Results are presented on the mean velocity field and the turbulent correlations by Laser Doppler Velocimeter, surface pressure distribution, surface temperature distribution, and thrust performance for two shroud geometries. The maximum primary nozzle pressure ratio tested was 3.0. The tests were conducted at primary nozzle temperature ratios of 1.0, 1.8 and 2.7. Two ejector characteristic lengths have been identified based on the dynamics of the ejector flow field, i.e., a minimum length L_m below which no significant mixing occurs, and a critical length L_c associated with the development of U'V' correlation in the ejector. These characteristic lengths divide the ejector flow field into three distinctive regions: the entrance region ($x<L_m$) where there is no direct interaction between the primary flow and the ejector shroud; the interaction region ($L_m<x<L_c$) where there is an increased momentum of induced flow near the shroud surface; and a "pipe" flow region ($L_c<x$) characterized by an increased skin friction where x is the distance downstream from the ejector inlet. The effect of the coflowing induced flow has been shown to produce inside the ejector a centerline velocity that has increased over the free-jet data. The normalized turbulent correlations are found to be 25 percent lower than those in free jets. The effects of pressure ratio on the ejector flow field are small. Present measurements also show that the ejector performance was not influenced by the primary nozzle temperature ratio up to 2.7.

TABLE OF CONTENTS

LIST OF TABLES

LIST OF FIGURES

NOMENCLATURE

C_p	$\frac{P-P_{amb}}{(\frac{1}{2}\rho U^2)_{ex}}$ Surface pressure coefficient
b	Blue laser beam
C	$\frac{\dot{m}\ measured}{\dot{m}\ isentropic}$; Primary nozzle discharge coefficient
d	Primary jet width
$\overline{D}$	Particle size
D	Laser beam diameter
g	Green laser beam
H	Ejector width
h(x)	Shroud width, = H for constant area ejector
L	Mixing chamber length
L'	Diffuser length
L_m	Length of entrance region
L_c	Ejector length for maximum velocity correlation. First to reach the wall
$\dot{m}$	Mass flow rate
M_{ex}	Primary jet exit Mach number
n	Complex index of refraction
p	Static pressure
P_r	P_o/P_{amb}; pressure ratio
P_{amb}	Ambient pressure
q_j	Dynamic pressure
R	Leading edge radius
Re	Reynolds number
S	Facility span
t_r	Primary nozzle temperature ratio

$t_r(\xi)$	Ejector shroud surface temperature ratio
T_E	Ejector thrust
T_o	Primary nozzle thrust
$\langle u \rangle$	Ensemble average
U	Velocity component in the x direction
U_G, U_B	Velocity component measured by the green and the blue beams respectively
U_{ex}	Primary jet exit velocity
$U_c(x)$	Centerline velocity
U'	r.m.s. value of the U velocity component fluctuation
V	Velocity component in the y direction
V'	r.m.s. value of the V velocity component fluctuation
$\overline{U'V'}$	Velocity correlation
X	Ejector shroud downstream location
x, y	Coordinates
β	Diffuser half angle
λ	$\frac{h(x)\int U^2 dy}{(\int U dy)^2}$; Profile uniformity parameter
$\overline{\lambda}$	Wavelength of light
ξ	Downstream distance measured from the mixing chamber entrance
ρ	Density
μ	Air viscosity
α	$\pi\ \overline{D}/\overline{\lambda}$, size parameter

Superscripts and Subscripts

-	Mean value
o	Stagnation conditions
ex	Primary jet exit conditions
amb	Ambient static conditions

I. INTRODUCTION

The jet thrust augmentation of an ejector system is governed by certain fluid mechanics phenomena associated with the entrainment of surrounding atmospheric air by the primary jet flow and subsequent mixing of this entrained fluid with the primary jet. Previous research has provided considerable insight into the operation of ejectors[1,2,3]. These studies have shown that the ejector thrust augmentation results from the low pressure on the shroud entrance region caused by entrainment of secondary fluid. Pressure recovery is achieved by turbulent mixing between the primary jet and the secondary stream. The use of a diffuser further enhances thrust augmentation by reduction of the entrance pressure. Ultimately, these flow processes result in a pressure distribution on the shroud and primary nozzle surfaces. The integrated effect of the pressure forces over these surfaces gives a positive contribution to the system thrust. The fundamental processes that relate entrainment, mixing, and diffusion with the pressure distribution on the ejector shroud and primary nozzle surfaces are not adequately understood and are some of the main objectives of the present research.

Large-scale testing and aircraft development programs which incorporate thrust augmenting ejectors have identified a number of problem areas which must be solved to achieve full implementation of the ejector concept in V/STOL applications[4,5]. Among them is the requirement for high augmentation within the limited volume available in high performance aircraft which results in insufficient mixing and in flow separation. Although ejector geometry is the primary design variable, from a fluid mechanics point of view it is valuable to relate these problems to the shroud surface pressure distribution and turbulent characteristics of the primary jet. For example, flow separation results from the inability of the boundary layer to manage a large adverse

pressure gradient encountered in a compact high performance ejector design. It can be prevented using suitable boundary layer control devices[6]. In order to determine the need of these control devices and to optimize their design, more quantitative information is necessary on the flow processes near the shroud surfaces.

For a given geometrical configuration insufficient mixing implies that there is insufficient energy transfer between primary and secondary flow with corresponding penalties in performance. Since the velocity distribution at the entrance section of the ejector is not uniform, it is important to quantify the combined effects of pressure gradient and turbulent structure on the downstream evolution of the velocity distribution. Qualitatively, the effect of adverse pressure gradient tends to increase flow non-uniformities while the effect of turbulent mixing is to reduce them[1]. Consistent with this qualitative argument is the increased performance found with hypermixing nozzles[6,7] and pulsatile primary jets[8].

An important aspect of thrust augmenting ejector operation is the influence on performance of primary flow total pressure and temperature. There is extensive literature on the effects of pressure ratio across the primary nozzle on ejector performance at ambient total temperature[2]. In contrast, there is little information available on the effect of primary flow total temperature. This information is limited to overall system performance and ejector shroud surface pressure distribution. There is no information however on the effect of these parameters on the turbulent structure within the ejector.

A number of mathematical models have been used to investigate ejector flows. One-dimensional analysis is useful in evaluating performance trends associated with changes in the geometrical configuration[9,10] and thermodynamic parameters of the ejector system[11]. The effect of the efficiency of

individual elements on overall system performance has also been investigated using one-dimensional analysis[6,12]. Other studies include phenomenological models[13-16] and finite difference algorithms [17,18]. The latter provide great flexibility in analyzing complex inlet geometries. The development of mixing is incorporated through suitable turbulence modeling. Detailed measurements of the ejector flow field including measurements of the turbulent quantities are required to evaluate the accuracy of these models [3].

An experimental research program was initiated at the JPL Fluid Dynamics Group to investigate the fluid dynamics of thrust augmenting ejectors. The objectives of this research are:

(A) To determine the role of the entrained fluid and its mixing with the primary jet on the shroud surface pressure distribution and on ejector performance.

(B) To measure the evolution of the various profiles and determine the effect of the confining shroud surfaces on their evolution.

(C) To determine the effect of primary flow total pressure and temperature on the flow characteristics within the ejector and on its thrust performance.

(D) To provide basic data to support analytical research.

The emphasis in this investigation is on the basic fluid dynamics phenomena which influence the thrust augmentation performance of an ejector. The ejector configuration chosen consists of a primary two-dimensional jet discharging into a rectangular ejector shroud. Simple shroud geometries are being used in order to minimize instrumentation difficulties. They are a constant area ejector and a constant area mixing chamber followed by a diffuser. Measurements of the system thrust, shroud surface pressure distribution, mean velocity field, and turbulent stresses field are reported.

The velocity measurements were obtained using a two-component Laser Doppler Velocimeter. The technique has been used based on the grounds: 1) It is non-intrusive, 2) does not require calibration, 3) can measure velocity in reverse flow regions, and 4) has been used successfully to measure the velocity field in flows with large temperature gradients[19]. Hot Wire Anemometry, the only available alternative, has never been successfully used in non-uniform temperature flow fields. Furthermore, probe calibration is required for velocity magnitude and direction; probe interference at the shroud can significantly influence the results of the measurements, and does not give direction discrimination in reverse flow regions. However, Laser Doppler Velocimetry requires the flow to be seeded with particles. Thus proper seeding devices must be built into the flow facility and the effect of particle concentration and size on measurement accuracy needs to be evaluated.

This report includes results obtained in two different ejector shroud geometries. It is organized as follows: The flow facility and instrumentation are described in Section II. A significant part of this section is devoted to the Laser Doppler Velocimeter. A detailed description of the system, data acquisition and data processing techniques is presented. The results described in Section III include measurements of the ejector configuration and free primary jet as well. When possible, the results of different measurements are compared against each other to verify their accuracy. The results are discussed in Section IV followed by a summary in Section V.

II. FLOW FACILITIES AND INSTRUMENTATION

Two different ejector facilities were designed and assembled during the course of this program. The low temperature facility was designed first. The description of the low temperature facility is given in reference (20) and will not be repeated here. In this report the high temperature facility will be described in detail. The details of the Laser Doppler Velocimeter and other instrumentation are presented.

2.1 Ejector Facility

The two-dimensional ejector facility was designed as shown in figure 1. The maximum primary nozzle pressure ratio of $P_o/P_{ex} = 4.0$ and stagnation temperature of 540°C can be obtained. A schematic diagram of the overall facility is shown in figure 2. A picture of the hardware is presented in figure 3.

Pressurized air from a compressor plant is used to drive the primary flow. A venturi tube, located in the supply line, directly measures the primary nozzle mass flow rate. Downstream of the venturi a combustor is used to elevate the temperature to the desired value by burning methanol. The facility is located in a test cell with adequate hot gas exhaust and breathing orifices on the side walls and ceiling in order to prevent recirculation of the hot gas inside the room. The ejector facility is mounted on linear bearings to accommodate thermal expansion of the pipes and to measure the system thrust. Flexible stainless steel hoses were used to couple the primary nozzle with the supply line to facilitate the thrust measurements as shown in figure 3.

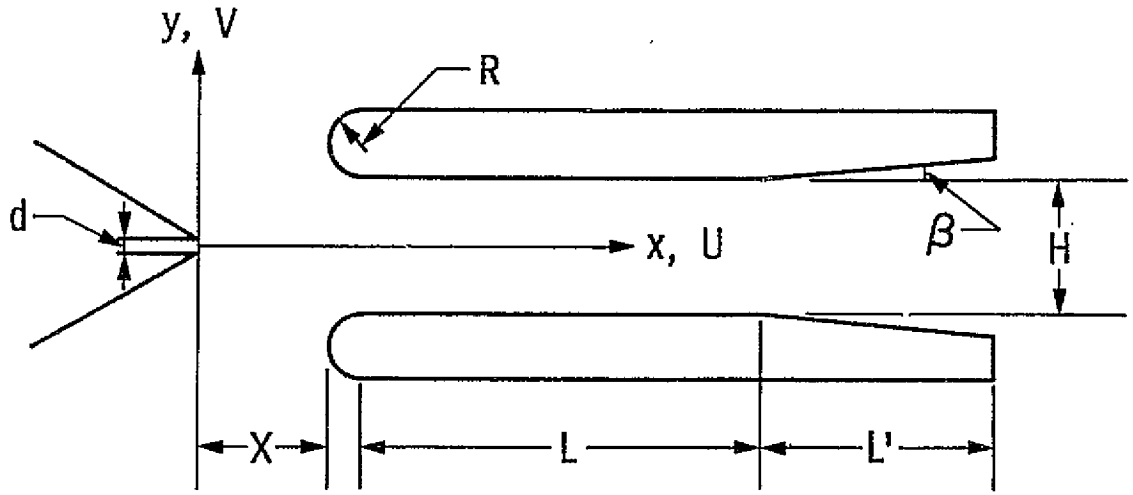

Figure 1. Thrust Augmenting Ejector Geometry

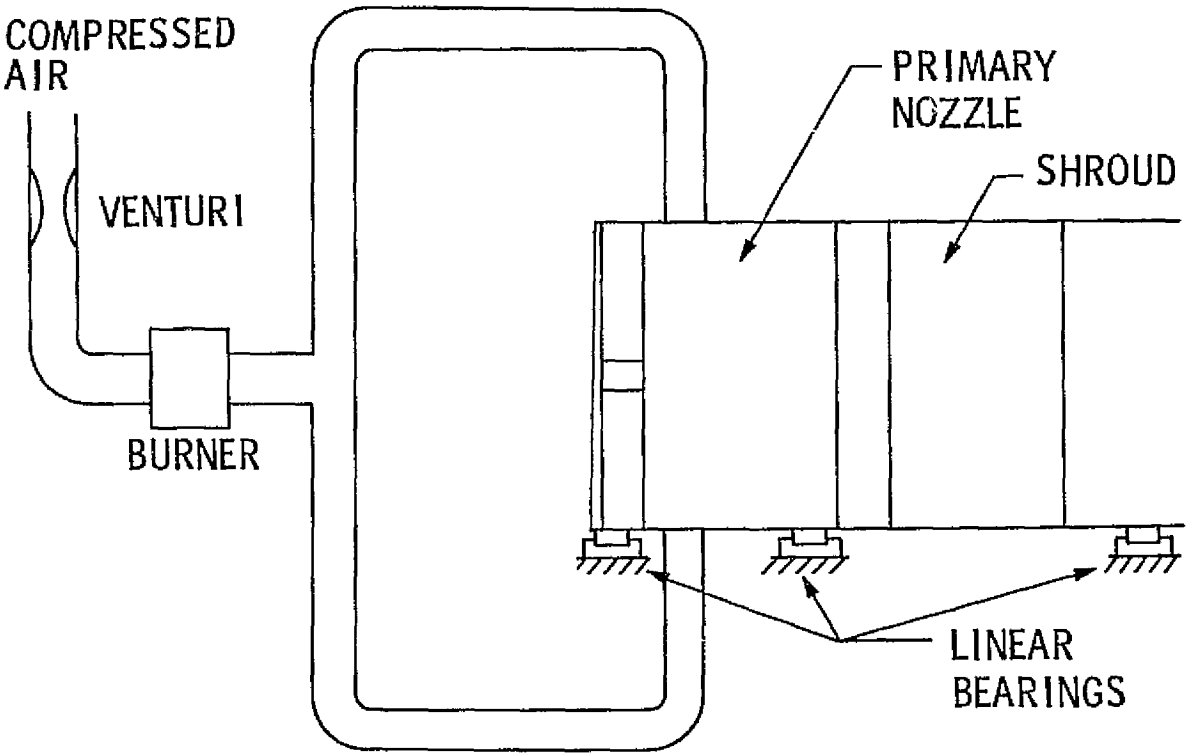

Figure 2. Schematic Diagram of the Ejector Facility

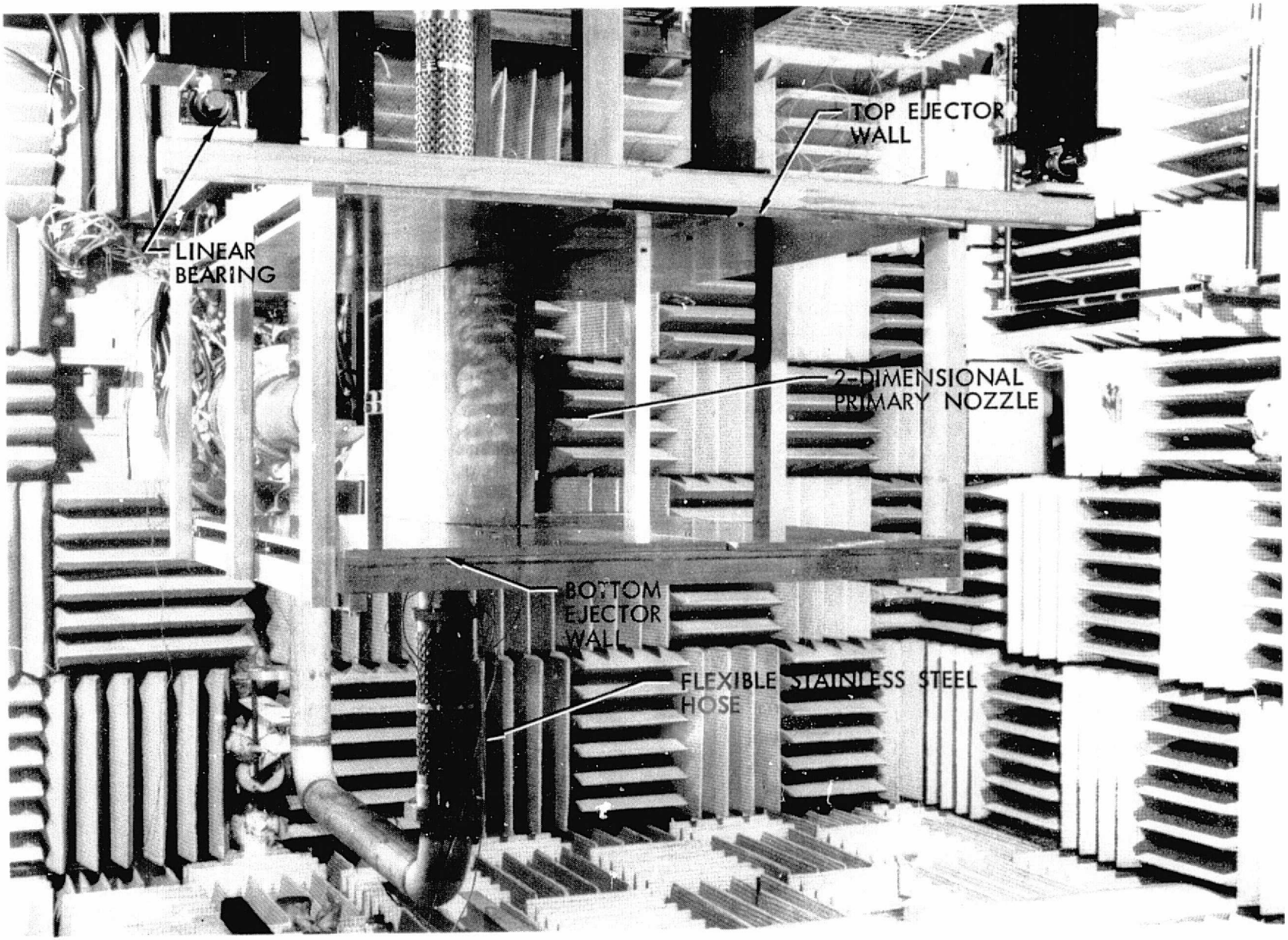

Figure 3. Ejector Facility

The primary nozzle is a slot-type two-dimensional nozzle. The exit area is rectangular 0.762 cm x 50.8 cm, the larger dimension being along the span of the nozzle. Several elements of the primary nozzle are shown in figure 4. The gas flow is fed into a stagnation section via a perforated tube. After a perforated plate and two stainless steel screens the flow enters the contraction section. The contraction is two-dimensional with an area ratio of 20 to 1. The internal contour of the contraction is formed by two circular arc sections as indicated in figure 4. The external surface of the nozzle is also contoured to provide a smooth flow path for the induced flow. Two large end plates are used to confine the flow in the spanwise direction. These plates are also used to support the shroud walls.

Two shroud geometries have been tested in this program. The geometrical parameters defining each one of them are presented in Table 1 (see figure 1 for the nomenclature. One of the ejector walls is instrumented with pressure taps along the mid-span plane as shown in figure 5. The other shroud surface is instrumented with two pressure taps and several thermocouples (figure 5). The shroud walls are attached to the end plates by a clamping mechanism which

Table 1. Ejector Geometry

	Constant Area	Diffused Flow
d(m)	7.62×10^{-3}	7.62×10^{-3}
H(m)	0.102	0.102
L(m)	0.305	0.305
L'(m)	-----	0.203
X(m)	0.102	0.102
R(m)	0.025	0.025
β(degree)	-----	5
S(m)	0.508	0.508

permits continuous adjustment of the location of the shroud relative to the primary nozzle. Proper alignment of the shroud walls relative to the nozzle

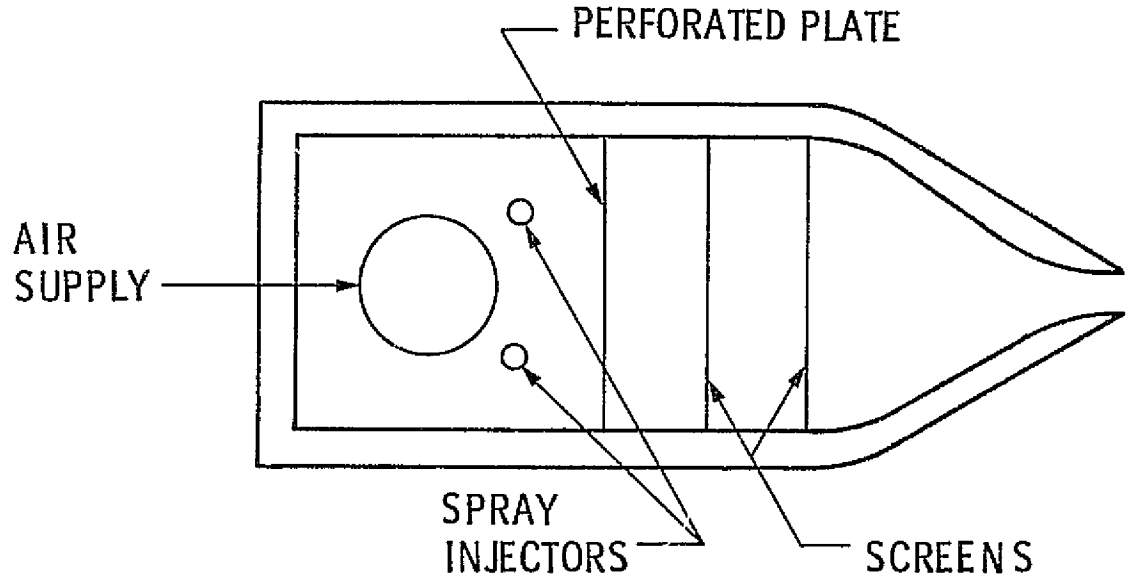

CONTRACTION AREA RATIO 20:1
EXIT AREA 0.3" x 20"
MAXIMUM PRESSURE RATIO 4
MAXIMUM TEMPERATURE 1000^{o}F

Figure 4. Primary Nozzle Geometry

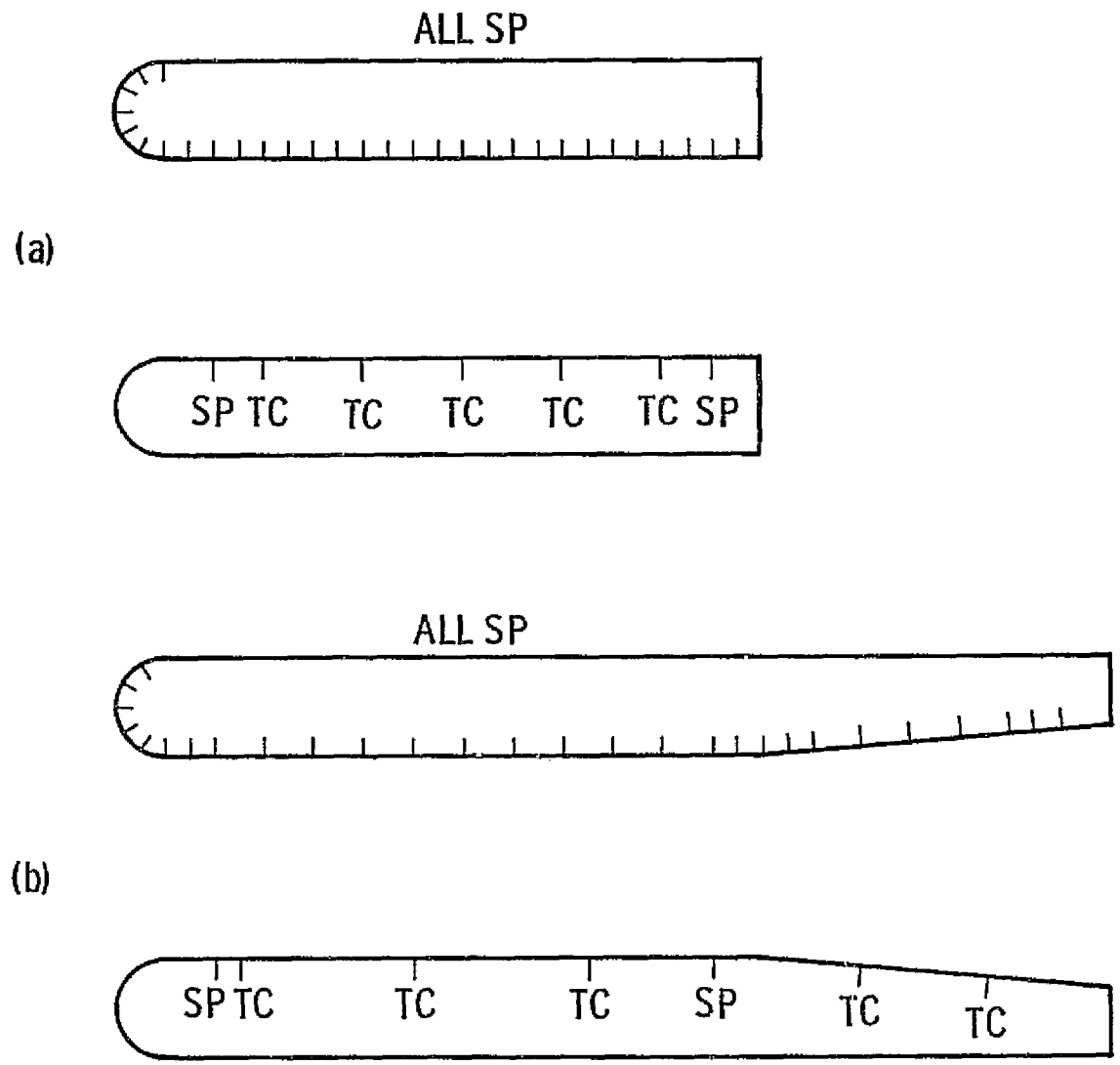

Figure 5. Ejector Shroud Geometry and Instrumentation (a) Constant Area Ejector (b) Diffused Flow Ejector

was obtained using the pressure taps on both shroud walls. The shrouds were considered aligned when the static pressure difference between the two walls measured at the same downstream position was smaller than 1 percent of the local gauge pressure.

2.2 Laser Doppler Velocimeter

The velocity field in the ejector was measured with a Laser Doppler Velocimeter (LDV). A commercially available two-component, two-color system LDV system was employed. The final experimental configuration was chosen after performing a large number of tests in the low temperature facility.[20] These tests were conducted in order to obtain the optimum performance characteristics by varying the optical system, analog processing, seeding materials, and processing software. A picture of the system in its final configuration is shown in figure 6. Forward scatter configuration has been used to reduce the dependance of the scattered signals on the complicated lobe structure of the Mie distribution, particularly in highly turbulent flows. When the particles that cause scattering are in the range $\frac{0.6}{n} < \alpha < 5$, where α is the size parameter and n the complex index of refraction, light scattering is adequately described by the Mie theory. The intensity distribution of the scattered light from such particles, termed the Mie distribution, is smooth in the forward direction and complicated in the back-scattering. The analog processors were operated in the single burst mode which suits the ejector application, since it requires low particle density seeding.

2.2.1 Optical system

The optical system used in this experiment is a forward scatter system, i.e., the receiving optics is located in the direction of propagation of the beams. Thus the transmitting and receiving optics are located at opposite

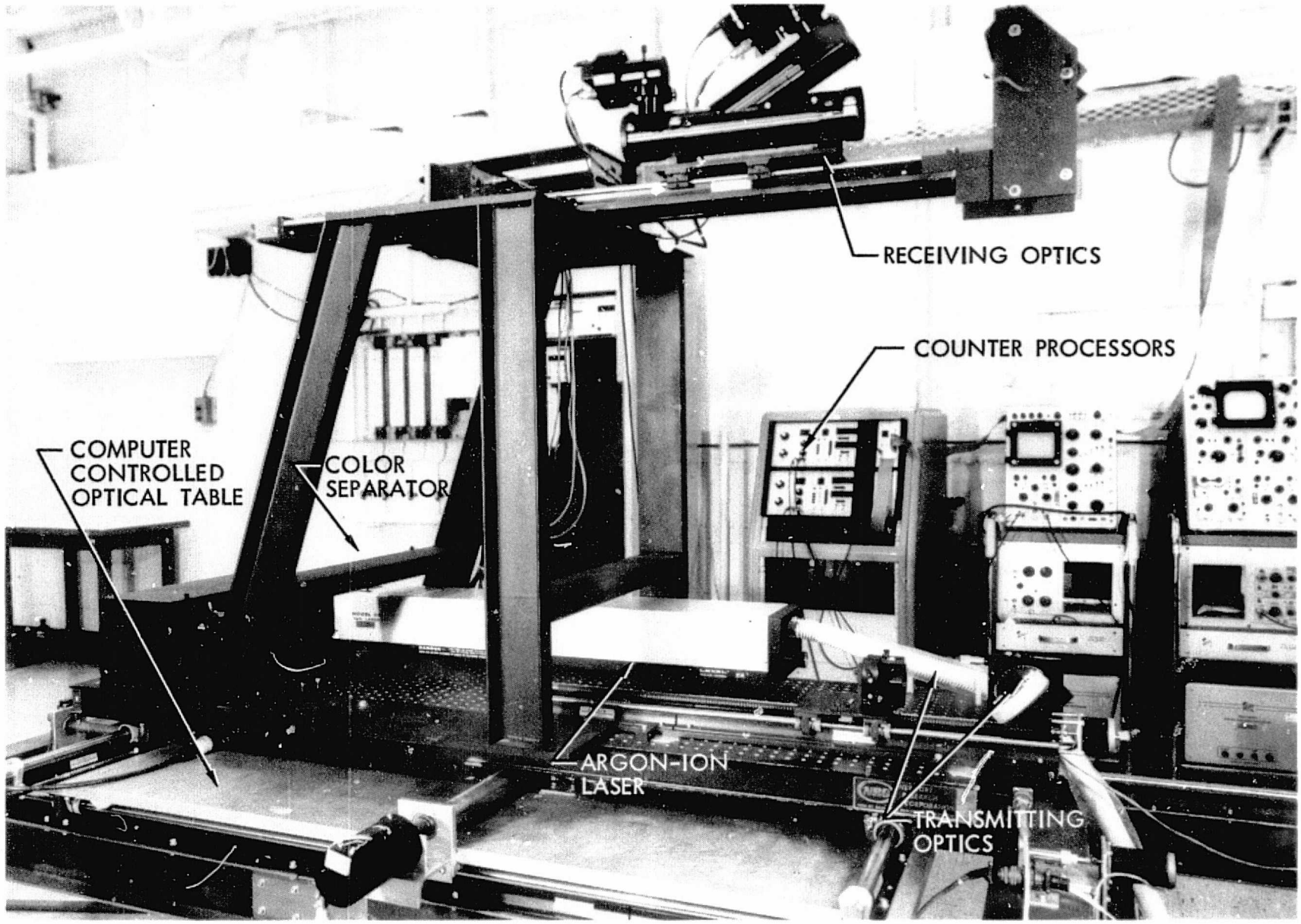

Figure 6. Laser Doppler Velocimeter (LDV)

sides of the facility as shown in figure 7. A schematic diagram of the transmitting optics is given in figure 8. A two watt argon-ion laser is used as the light source. Past a collimating lens, a color separator provides two lines of the laser, the 514 nm green line and 488 nm blue line. Each beam is split into a pair of equal intensity beams by a polarization rotator and a beam splitter. A single 598 mm focal length lens is used to form the measuring volume which contains the overlapping focal volumes of the blue and the green beams. A flat first surface mirror is used to rotate the beams 90°, thus the measuring volume is formed in the test section as shown in figure 7.

The receiving optics components are shown schematically in figure 9. The scattered light from the particles is collected by a 761 mm focal length lens after reflection from a mirror. A dichroic mirror is used to separate the components of each color. Finally, the scatter light of each color is focused into a pin hole (250 μm) and photomultiplier tube assembly.

The component of the velocity vector measured by the LDV and the Doppler constant used to convert frequency into velocity vector are determined by the transmitting optics. A diagram of the fringe formation is shown in figure 10. The fringes in the green focal volume form an angle of -45° with the downstream direction and, therefore, the velocity component measured by the green beams forms an angle of +45° with that direction. Similarly the blue beams measure the velocity component forming an angle of -45° with the downstream direction. The Doppler constant which is related to the fringe spacing in the focal volume is given by the equation

$$K = \frac{\lambda}{2 \sin \frac{\Theta}{2}} \qquad (1)$$

where λ is the light wavelength and Θ=4.72° gives Doppler constants for the green and blue velocity components K_g = 6.24 (m/sec)(MHz)$^{-1}$ and K_b=5.92

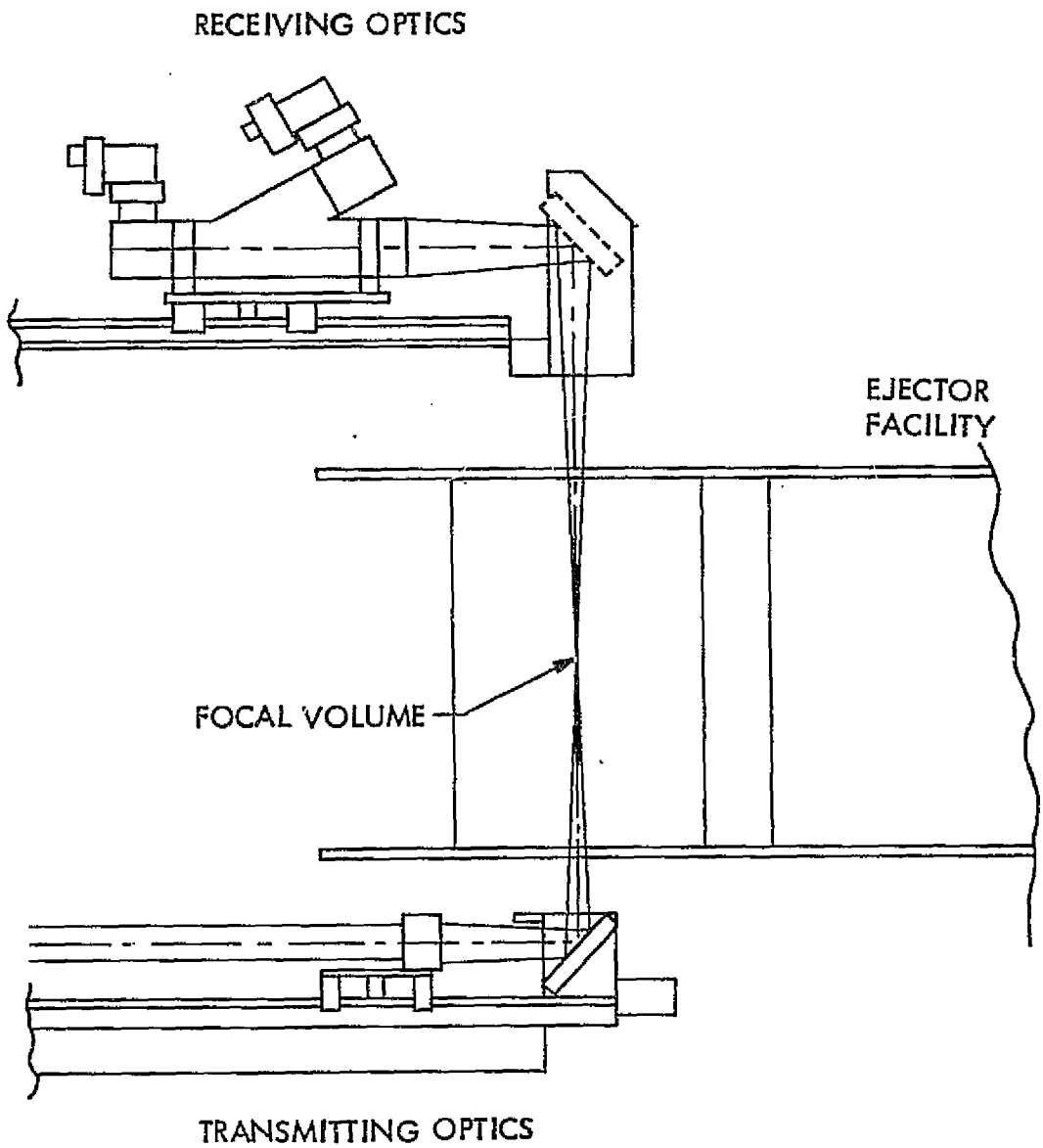

Figure 7. LDV Location Relative to the Test Section

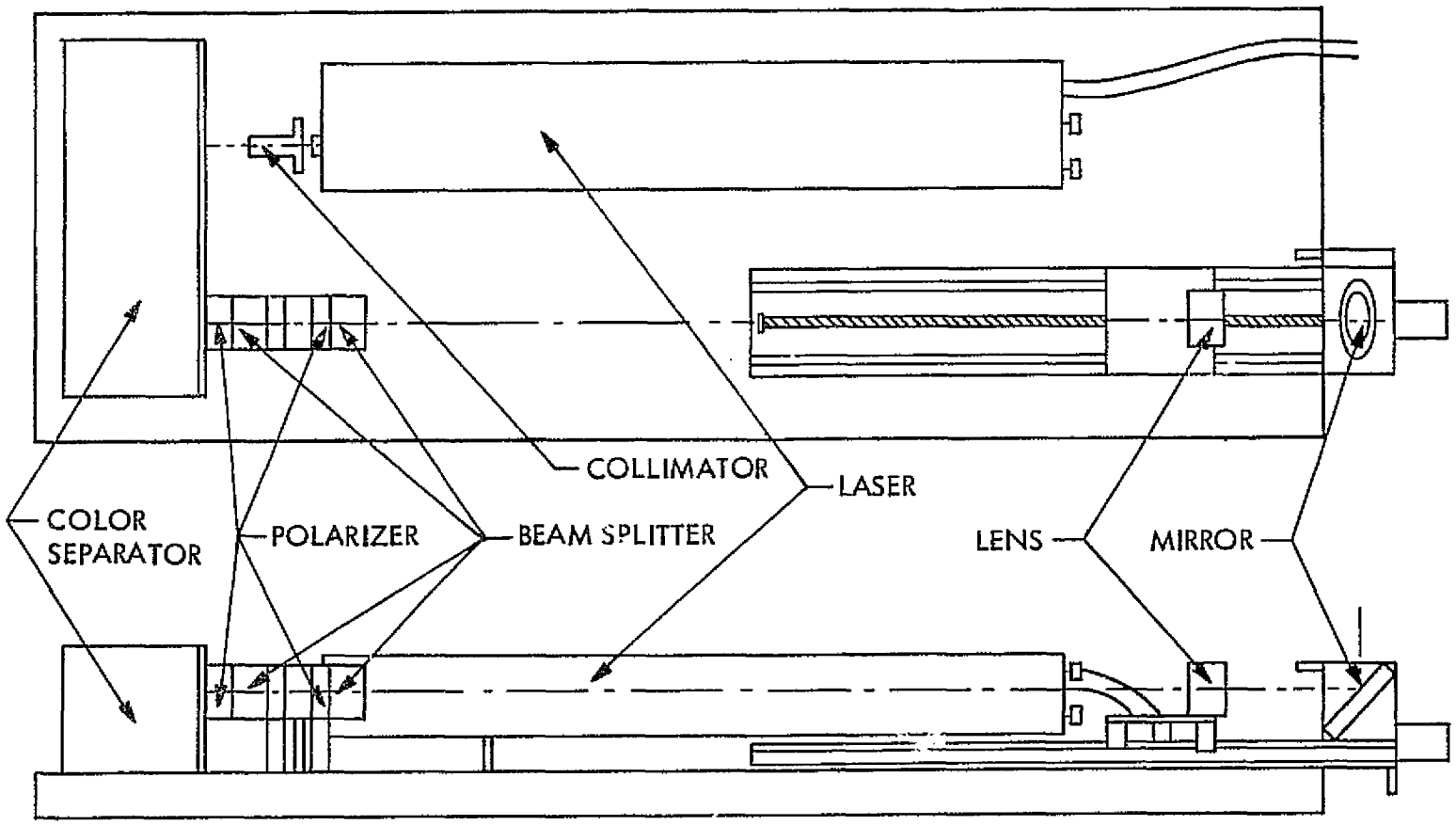

Figure 8. Transmitting Optics Schematic

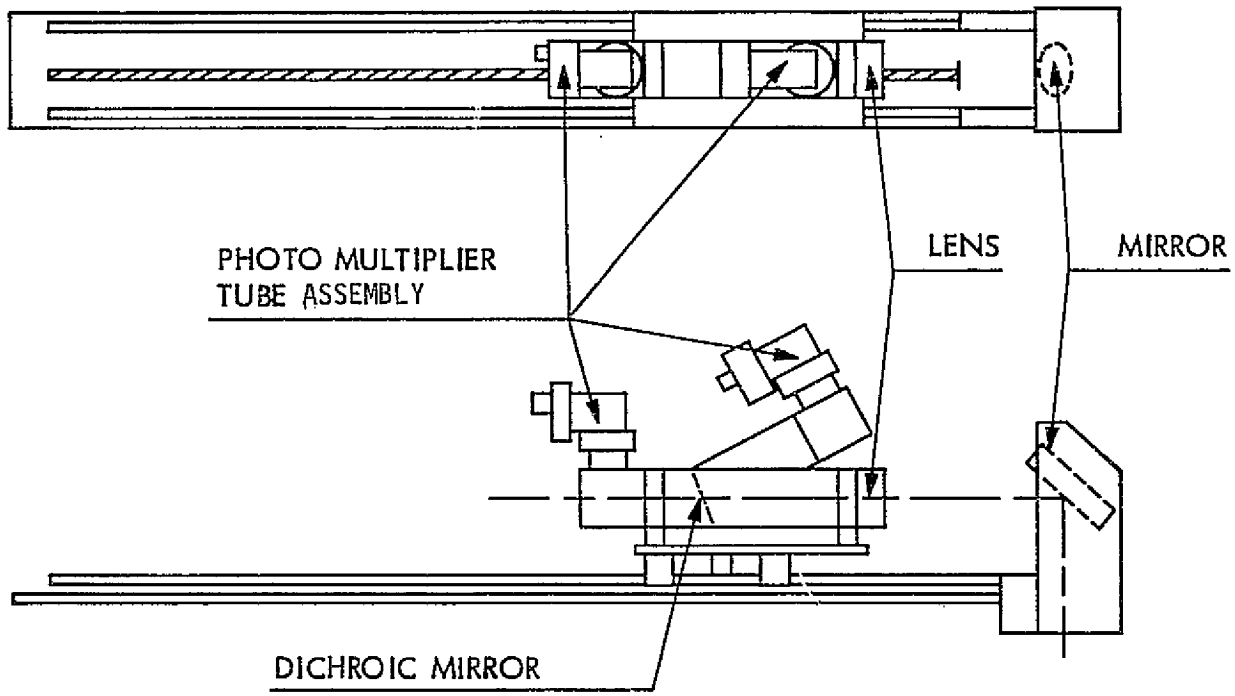

Figure 9. Receiving Optics Schematic

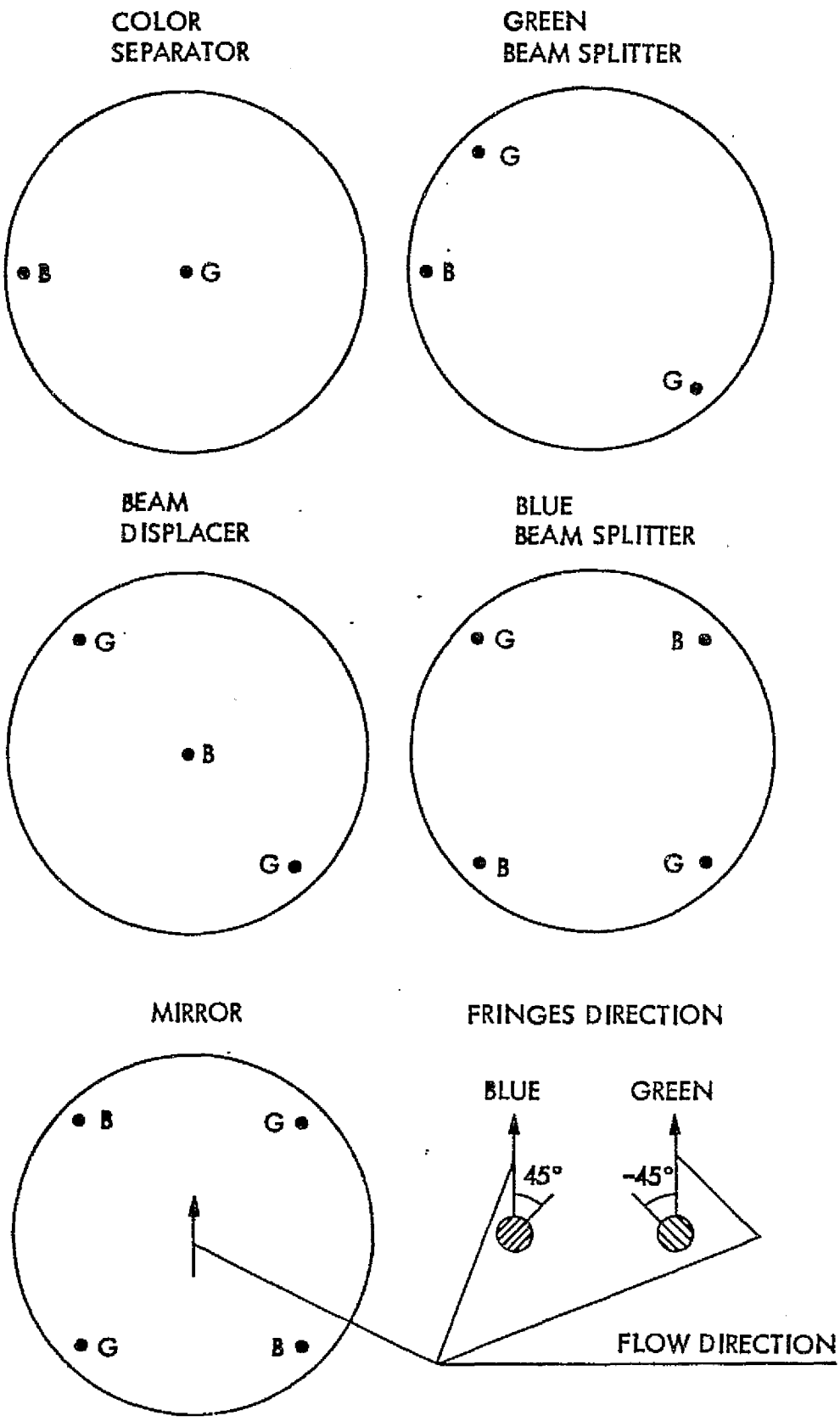

Figure 10. Focal Volume Formation Schematic

$(m/sec)(MHz)^{-1}$ respectively. The detailed geometrical characteristics of the focal volume are given in Table 2.

The entire LDV hardware is mounted on an optical table that can be moved by means of remotely operated stepping motors. Motion of the focal volume on a fixed span plane was obtained by the horizontal displacement of the optical table. Motion along the span resulted from the displacement of the focusing lens and the receiving optics along their optical axis. The table can be moved in steps of 2.5 mm, with an absolute accuracy of 100 μm.

Table 2. Laser Doppler Velocimeter Focal Volume Characteristics

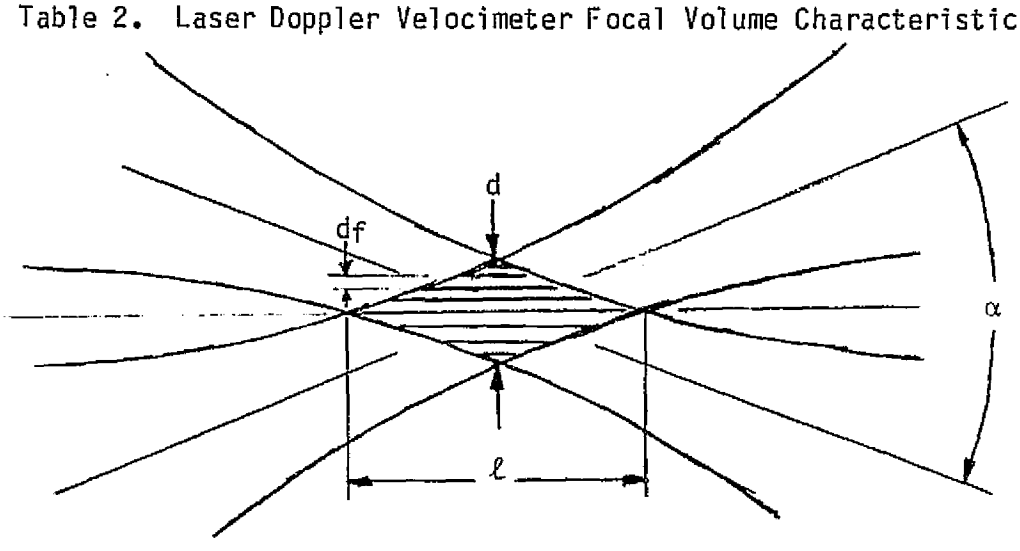

Lens focal length, f = 598 mm

Beam crossing angle, α = 4.72°

Beam diameter, D = 1.3 mm

Focal volume length*, ℓ = 7.3 mm

Focal volume width*, d = 0.3 mm

Fringe spacing*, d_f = 6.1 μm

Number of fringes, N_{fr} = 48

*These values are mean and vary by 5% for the blue and the green focal volumes.

The optical configuration just described can be used to measure the velocity field only at distances from the shroud wall greater than 1 cm. At shorter distances the two beams are interrupted by the shroud as they enter the test section, thus preventing the formation of the focal volume. Measurements close to the shroud wall were made by operating the LDV in a single component configuration. In this case, the green beams were positioned on a plane parallel to the shroud wall; therefore, only the downstream component of the velocity was measured. Measurements as close as 0.25 cm from the wall were obtained.

2.2.2 Particle Generator and Injector

In order to measure the flow velocity with a Laser Doppler Velocimeter, the air flow must be seeded with particles. It is the velocity of the particles that is measured by the system. The objective of the seeding device is to provide a spatially uniform concentration of particles, their size small enough to follow the flow while providing sufficient scattered light for an adequate signal to noise ratio. The seeding technique used in the low temperature facility is described in reference 20. In the high temperature facility, silica particles were used. Their size distribution is shown in figure 11. The mean particle diameter is 1.55 μm which gives a terminal settling velocity of 0.019 cm/s or equivalently a response time of 19.4 μs.[21]

Both primary and induced flows were seeded with particles. A commercially fluidized bed aerosol generator was used to produce a highly concentrated aerosol, 10^5 particles/cm^3. The aerosol was introduced in the flow using spray bars of the same geometry as those used in the low temperature facility.[20] A schematic diagram of the aerosol injection system is shown

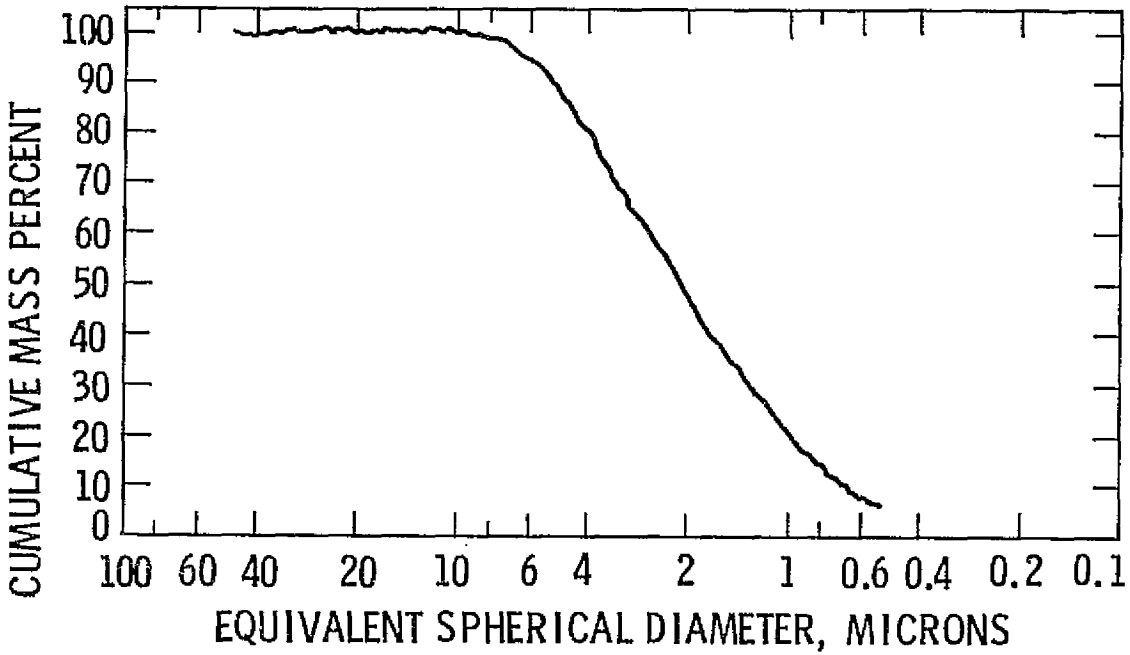

Figure 11. Particle Size Distribution

in figure 12. The primary flow is seeded in the stagnation section upstream of the perforated plate (figure 4). The induced flow spray bars are located upstream of a perforated plate and a screen in order to minimize the flow distortions (figure 13). As indicated in figure 13, the induced flow is confined into a large channel from the seeding point to the entrance to the shroud. The size of the channel is large enough to minimize its influence on the flow field.

2.2.3 Signal Processor and Data Acquisition

The measurement of the velocity can be obtained only after suitable processing of the photomultiplier tubes output as the scattering particles move across the focal volume. Two counter processors were used, one for each velocity component. They were operated in the single-burst mode, i.e., only one particle is present in the focal volume when the measurement is made. In addition, the system is operated in the coincidence mode in which the output of the processors is tested for coincidence in time so that the two components of the velocity vector as determined by the optical setup are measured on the same particle.

The signal processing is accomplished in four stages: analog processing, burst processing, coincidence test and transfer to the computer. The analog processing involves suitable filtering and amplification of the signal for optimum signal to noise ratio. Both high pass and low pass filters are used. The low pass filter is used primarily for pedestal removal and low frequency noise removal; low frequency noise is introduced by imperfections in the optical system. The cut-off values used varied from 300 kHz to 1 MHz depending on the flow velocity. The low pass filter is used for removal of high frequency noise. Cut-off values from 2 MHz to 100 MHz were used

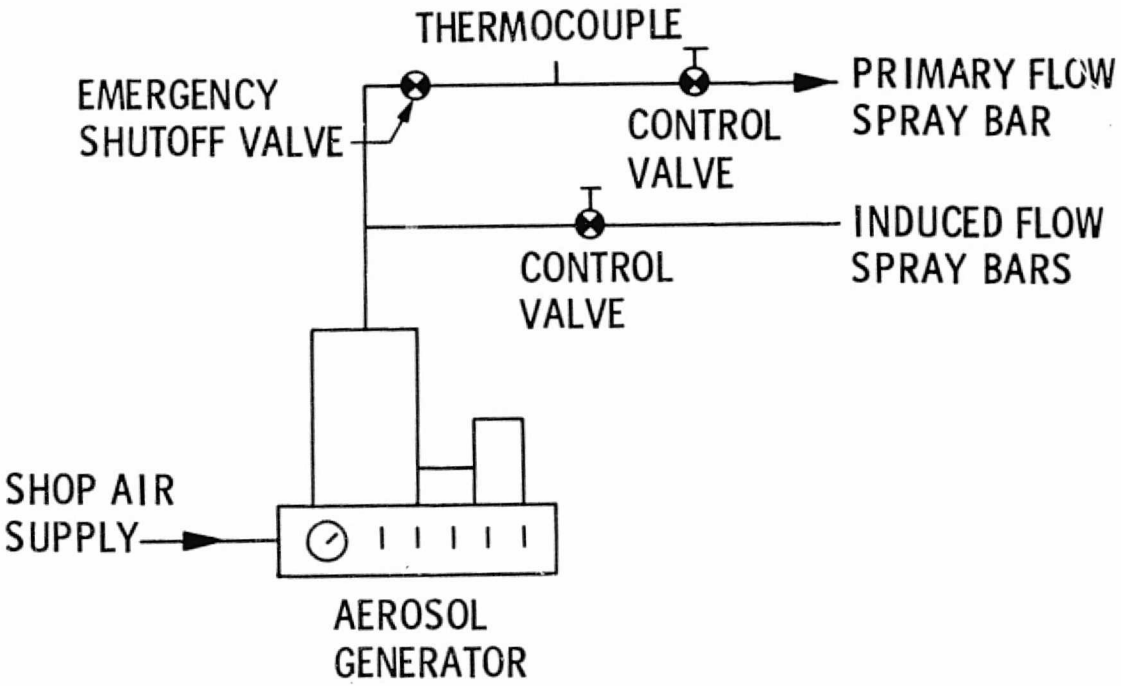

Figure 12. Particle Injection System

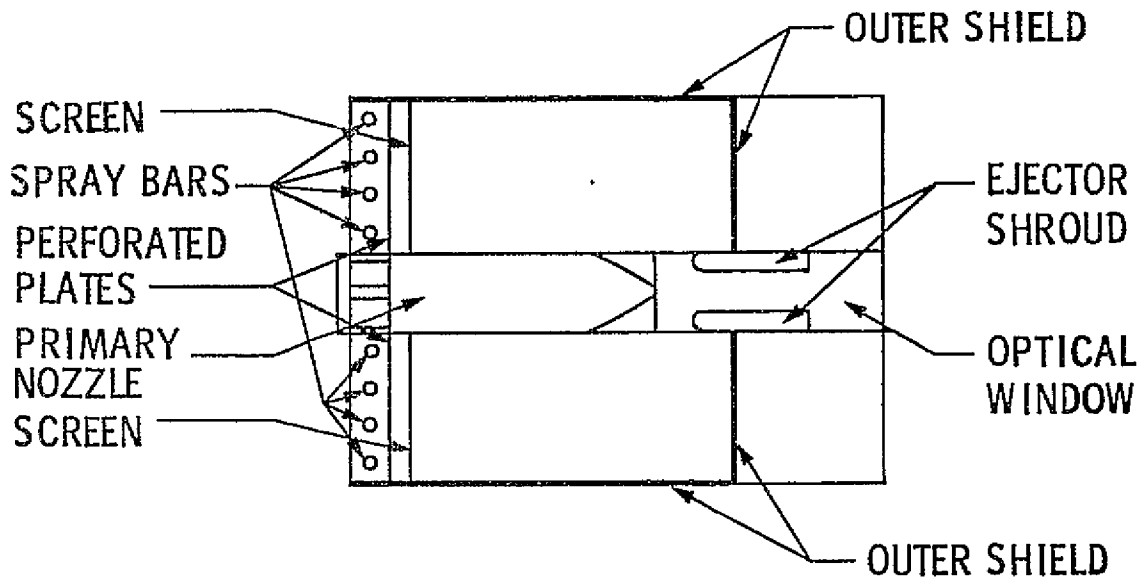

Figure 13. Induced Flow Seeding Schematic

depending on the flow velocity. The output of the filter is processed by an amplifier. In the present experiments however, the gain was set at unity, thus no amplification was needed for adequate operation of the system. Typical signal to noise ratio past the amplification stage was in excess of 100.

The burst processing encompasses the required electronics for the actual measurement of the particle velocity. A level detector determines the presence of a burst. Measurements are made of the total number of cycles in each burst, i.e., the number of fringes crossed by the particle, and its total time duration. The resolution of the time measurement is 1 nsec. Only bursts with more than 8 cycles are used for processing. The output of the burst processor is in digital form. It feeds into the computer interface that incorporates the coincidence test between the two processors. The coincidence test consists of the initiation of a time window after completion of processing by one of the processors. If data from the other processor is not received before the end of the window, the data is discharged; otherwise, coincidence is attained and the data from both processors is transferred to the computer. A time window of 17 μsec was used in all the experiments.

The Laser Doppler Velocimeter operates in conjunction with a minicomputer system. The data acquisition process is initiated by the minicomputer software after allocation of a suitable memory buffer. Data transfer from the signal processor to memory occurs under hardware control via Direct Memory Access until one of two conditions is satisfied: 1) The memory buffer is full, or 2) a specified elapsed time has passed (time-out). Preprocessing is then initiated on the resulting variable size buffer which involves search and removal of transmission errors, transformation of the data from signal processor format to Doppler frequencies, and computation of a frequency histogram

for each velocity component. The frequency histograms are displayed on the computer terminal in order to verify proper operation of the system. After preprocessing is completed, the data is transferred to magnetic tape for additional processing. The data buffer used in these measurements corresponds to 8,000 velocity measurements. The maximum elapsed time was specified as 60 seconds. These values are a compromise designed to minimize the uncertainty of the results while maintaining the total time of the experiment within reason. They also take into account the typical data rate.

Prior to every experiment utilizing the LDV system, several tests were conducted to verify adequate operation of the system, e.g., the transmitting optics alignment and overlapping of the green and the blue focal volumes. The fringes within the focal volumes were also inspected to prevent distortions and intensity non-uniformities. The alignment of the receiving optics was verified with the facility in operation. The high-pass and low-pass filters in the signal processor were set to predetermined values depending on the expected flow velocity. The gain of the amplifiers was adjusted for optimum signal to noise ratio. The flow rate through the aerosol generator was set for a data rate between 100 to 1000 particles per second. These data rates are consistent with the buffer size and maximum elapsed time used in the data acquisition software.

2.2.4 Data Processing

The velocity data generated in these tests were processed using the same minicomputer system used for data acquisition. Some valuable information was generated by the data acquisition software, namely the computation of the velocity histograms. The data processing software was designed to obtain the mean and first order correlations of the measured velocity components and to

transform these results to the physical frame of reference. In the computation of the mean velocity and correlations, a weighting factor is needed. Several possibilities were investigated as reported in reference 20. The conclusion of that study was that the uncertainty of the measurements will not be improved by using velocity bias correction. Therefore, equal weight averaging was used which results in a significant reduction of processing time. Thus the expressions used to compute the mean and correlations are

$$\overline{U_{G,B}} = \frac{1}{N} \sum_{n=1}^{N} (U_n)_{G,B} \tag{2}$$

$$\overline{U^2_{G,B}} = \frac{1}{N} \sum_{n=1}^{N} (U^2_n)_{G,B} \tag{3}$$

$$\overline{U_G\, U_B} = \frac{1}{N} \sum_{n=1}^{N} (U_n)_G \cdot (U_n)_B \tag{4}$$

where the subscripts G and B refer to the velocity measured by the green and the blue beams respectively.

A simple transformation relates the mean and the first order correlations of the measured velocity components with those in the x and y directions. This transformation is illustrated in figure 14. The equations relating the mean and correlation of the various velocity components are

$$\overline{U} = \overline{U_B} \sin\phi + \overline{U_G} \cos\phi \tag{5}$$

$$\overline{V} = \overline{U_B} \cos\phi - \overline{U_G} \sin\phi \tag{6}$$

$$\overline{U^2} = \frac{\overline{U^2_G} + \overline{U^2_B}}{2} + \frac{\overline{U^2_G} - \overline{U^2_B}}{2} \cos 2\phi + \overline{U_G\, U_B} \sin 2\phi \tag{7}$$

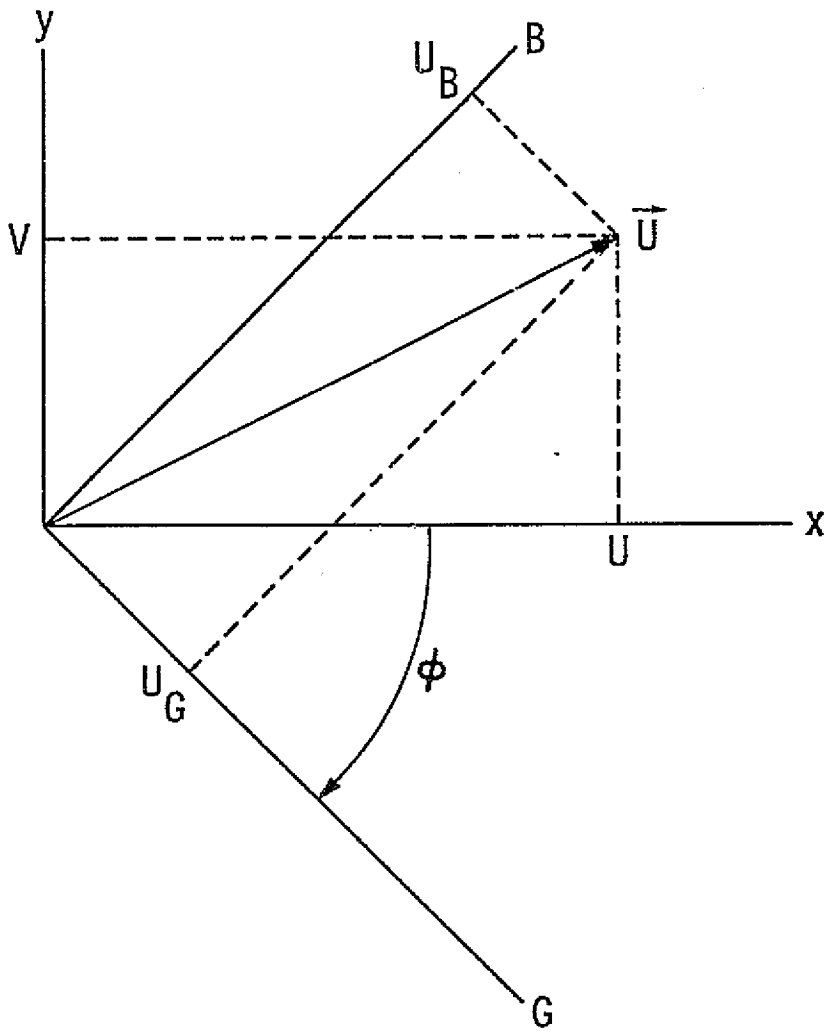

Figure 14. Velocity Transformation

$$\overline{V^2} = \frac{\overline{U^2_G} + \overline{U^2_B}}{2} + \frac{\overline{U^2_G} - \overline{U^2_B}}{2} \cos 2\phi - \overline{U_G U_B} \sin 2\phi \qquad (8)$$

$$\overline{UV} = \frac{\overline{U^2_G} - \overline{U^2_B}}{2} \sin 2\phi + \overline{U_G U_B} \cos 2\phi \qquad (9)$$

where ϕ is the angle between the direction of the velocity component measured by the green beams and the downstream direction, positive in the counter-clockwise direction. From these quantities, the rms value of the fluctuation of the U and V velocity components and their cross-correlation can be calculated using the following standard relationships:

$$U' = \overline{U^2} - \overline{U} \qquad (10)$$

$$V' = \overline{V^2} - \overline{V} \qquad (11)$$

$$\overline{U'V'} = \overline{UV} - \overline{U}\,\overline{V} \qquad (12)$$

The reproducibility of the measurements was better than 1 percent. The expected accuracy of the results was estimated as 2 percent for the measured velocity components. The accuracy of the velocity correlations was estimated as 10 percent. These estimates take into consideration several sources of uncertainty including the effects of velocity bias and fringe bias[22-24].

2.3 Other Instrumentation

In addition to the velocity measurements, the ejector flow field was documented with direct thrust measurements, primary nozzle mass flow rate measurements and surface pressure measurements. Pressure measurements were also used to monitor the operation of the primary nozzle. A number of

temperature measurements were made to monitor the primary nozzle total temperature and to characterize the ejector shroud surface temperature. The pressure measurements were made with strain gauge pressure transducers. Their accuracy is estimated at 0.1 percent of the measured value. The temperature measurements were made with type K thermocouples and commercial read-out units. Their accuracy is $\mp$ 1 degree centigrade.

Measurements of the primary nozzle air flow rate were made using a venturi tube. As indicated earlier, the venturi tube was located upstream of the combustor in the primary nozzle supply line. This mass flow was corrected due to addition of fuel for hot primary flow runs. The mass flow rate was obtained from measurements of the pressure and temperature upstream of the venturi and the pressure at the throat. One dimensional gas dynamics formulas were used to calculate the ideal mass flow rate. A mass flow coefficient was used to correct for real gas effects. Handbook values were used for the mass flow coefficient[25].

The surface pressure distribution on the shroud was measured at the points indicated in figure 5. Two pressure transducers and scanvalves were used for the upstream and downstream pressure taps respectively. An overlap of two pressure taps was used to verify proper operation of the system. The results of surface pressure measurement were processed using the minicomputer system. Computer software was developed to calculate the surface pressure coefficient. This software integrates the surface pressure around the leading edge and along the diffuser to calculate the contribution of the pressure forces on the shroud to the system thrust. The integrals were calculated using Simpson's rule.

Two different techniques were used for direct thrust measurements. In the low temperature facility a load cell was used. This system has been

described in reference 20. In the high temperature facility, however, a load cell could not be used because of thermal expansion. Instead, measurements were made using the system shown schematically in figure 15. In this technique the thrust of the system is balanced by the force acting on a piston. Measurement of the differential pressure across the piston determines the force acting on the system. Along with the force measurement, a linear potentiometer gives the position of the facility relative to the supply pipes. The assumption is made that there is a "zero" relative position at which the contribution to the measurement of forces acting on the supply pipes is negligible. Hence the measurement is made only when the facility is at this position. The reproducibility of the results is very good. However, due to uncertainties in the definition of the "zero" position as a function of supply pressure, only relative measurements are presented.

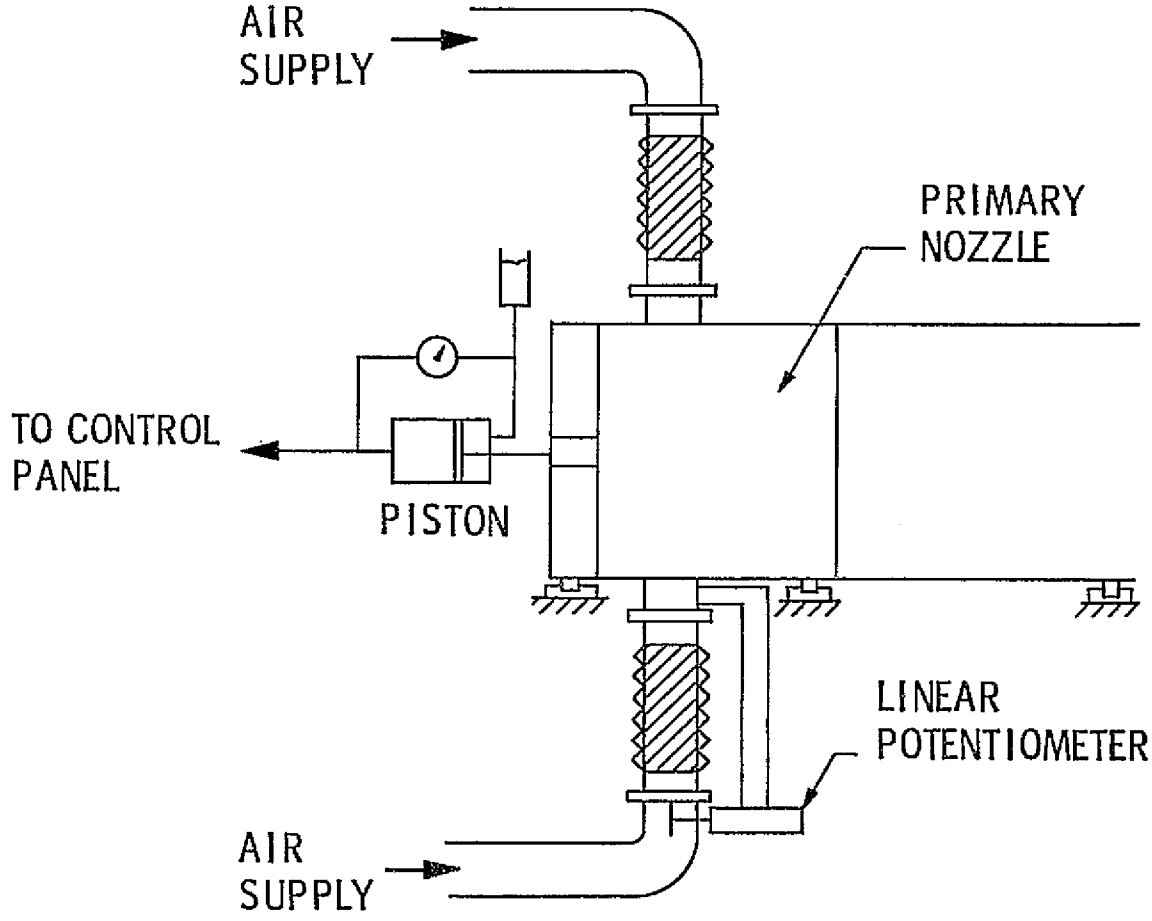

Figure 15. Thrust Measurement System

III. RESULTS

3.1 Facility Validation and Preliminary Results

Tests were conducted to determine the flow field characteristics and performance of the primary nozzle in both the low and the high temperature facilities. Pitot tube surveys were made in the low temperature facility to characterize the spanwise uniformity of the flow and to determine the free-jet characteristics. The spanwise variations of the jet exit velocity were found within 0.5 percent of the mean velocity. The free-jet results are presented in figures 16 to 18. The evolution of the normalized width of the jet is shown in figure 16. The jet width δ is defined as the distance between points where the velocity is one-half the local centerline velocity. As expected, the jet width increases linearly with downstream distance sufficiently far downstream. A least square fit to the data for $x/d>10$ gives

$$\frac{\delta}{d} = 0.19 \quad \frac{x-x_o}{d} \mp 0.19 \qquad (13)$$

where $x_o/d = 3.0$. The centerline velocity decay is shown in figure 17. The centerline velocity decays as $x^{-\frac{1}{2}}$ after the potential core. The self similar velocity decay was found to be

$$\frac{U_c}{U_{ex}} = 2.68 \quad \frac{x-x_o}{d}^{-\frac{1}{2}} \mp 0.005 \qquad (14)$$

Comparison of these data with the results of other investigations is made in figure 18. The continuous line on this figure was obtained from the results presented in reference 26, which cover the Reynolds number range up to $Re_d = 3.4 \times 10^4$ (c.f. $Re_d = 8.5 \times 10^4$ in the present measurements). The self-similar growth rate and centerline velocity decay are in agreement with the results of other investigations.[27-30] The location of the virtual origin (x_o) is also within the scatter of measurements.

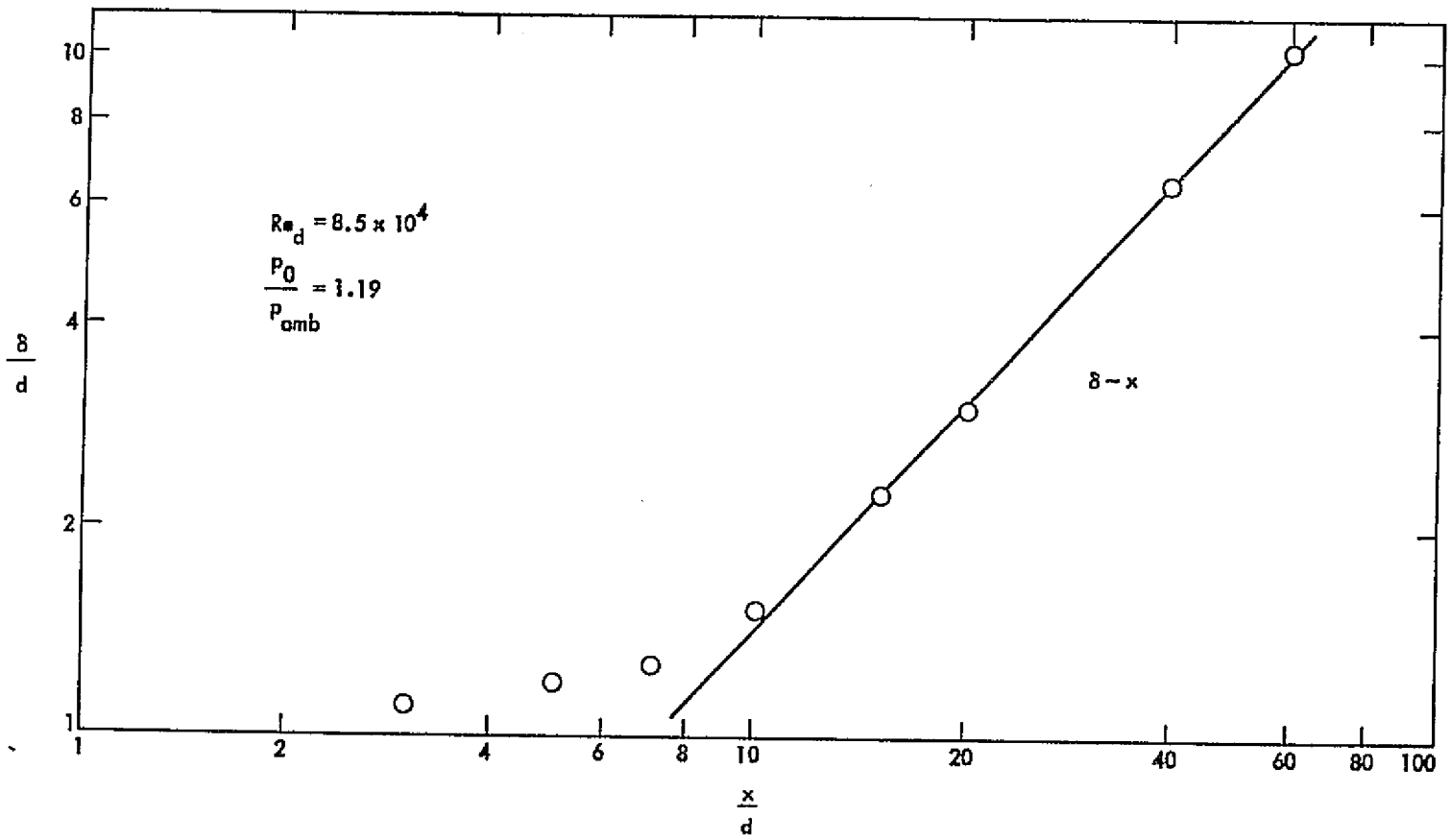

Figure 16. Free-Jet Growth

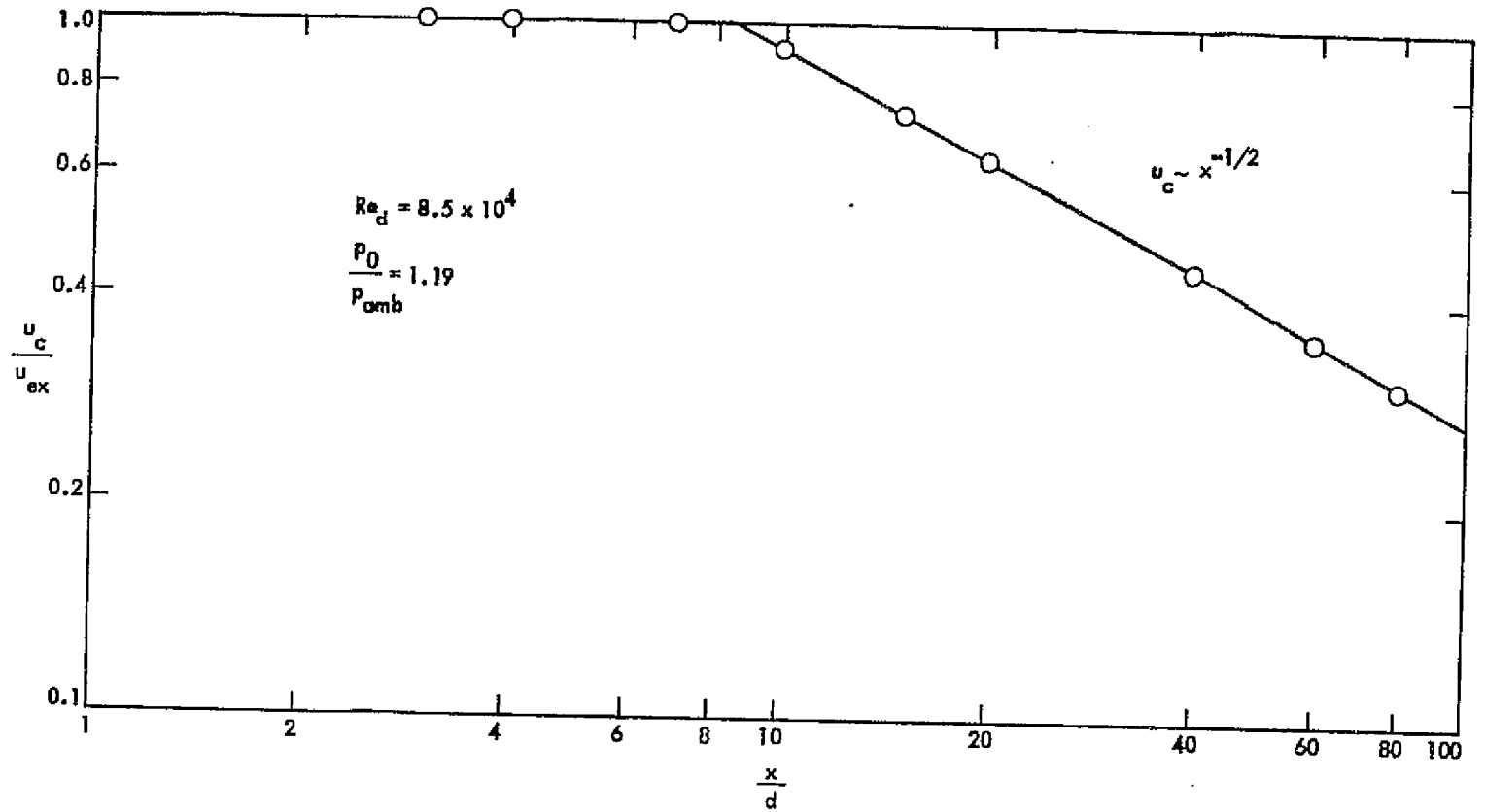

Figure 17. Centerline Velocity Decay

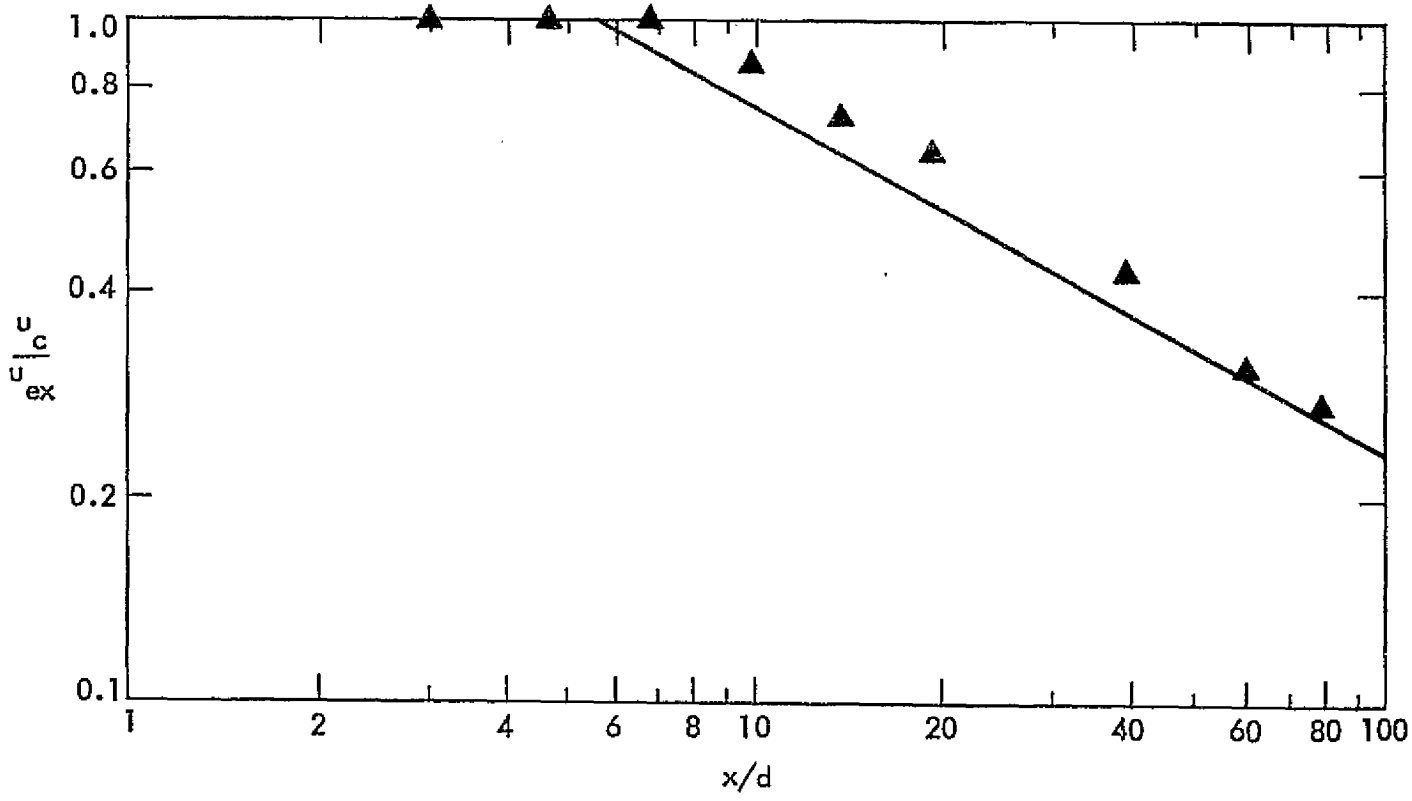

Figure 18. Centerline Velocity Decay. Comparison with Collected Data on Reference 25.
▲ Present Results; Solid Line, Reference 25

The tests conducted in the high temperature facility were limited to spanwise surveys of the pressure and temperature, and measurements of the mass flow coefficient of the nozzle. The spanwise uniformity of the total pressure and temperature were found better than 0.5 percent of the mean. The mass flow coefficient results are presented in figure 19. The mass flow coefficient C_V defined as the ratio of the measured mass flow rate of the nozzle to the ideal one-dimensional mass flow rate, is plotted as a function of nozzle exit Reynolds number ($Re_d=\frac{\bar{m}}{S\mu}$) at temperature ratios t_r =1.0, 1.85 and 2.73. At sufficiently high Reynolds number and temperature ratios of 1.85 and 2.73, these results show a mass flow coefficient greater than one. Although it may seem striking, mass flow coefficients greater than one have also been reported in axisymmetric configurations[31-34]. They are the result of the negative boundary layer displacement thickness which is caused by the combined effects of heat transfer and rapid flow acceleration.

The ejector configurations investigated were chosen after analysis of several preliminary tests on constant area ejectors at primary nozzle exit Mach numbers from M_{ex}=0.2 to 0.7. Tests were first conducted with an ejector shroud of area ratio 16.7, a leading edge radius of 3.8 cm, and a mixing chamber length of 30.5 cm. This configuration did not produce any thrust augmentation, irrespective of the ejector shroud location relative to the primary nozzle, to a maximum value of X/H=1. Flow visualization showed that within the range of the Mach number tested, a reverse flow region existed on one shroud surface while the flow remained attached to the other surface. The particular shroud surface on which the flow remained attached appeared to depend on conditions at the leading edge of the shroud. However, after the flow was established, the wall at which the flow remained attached could be

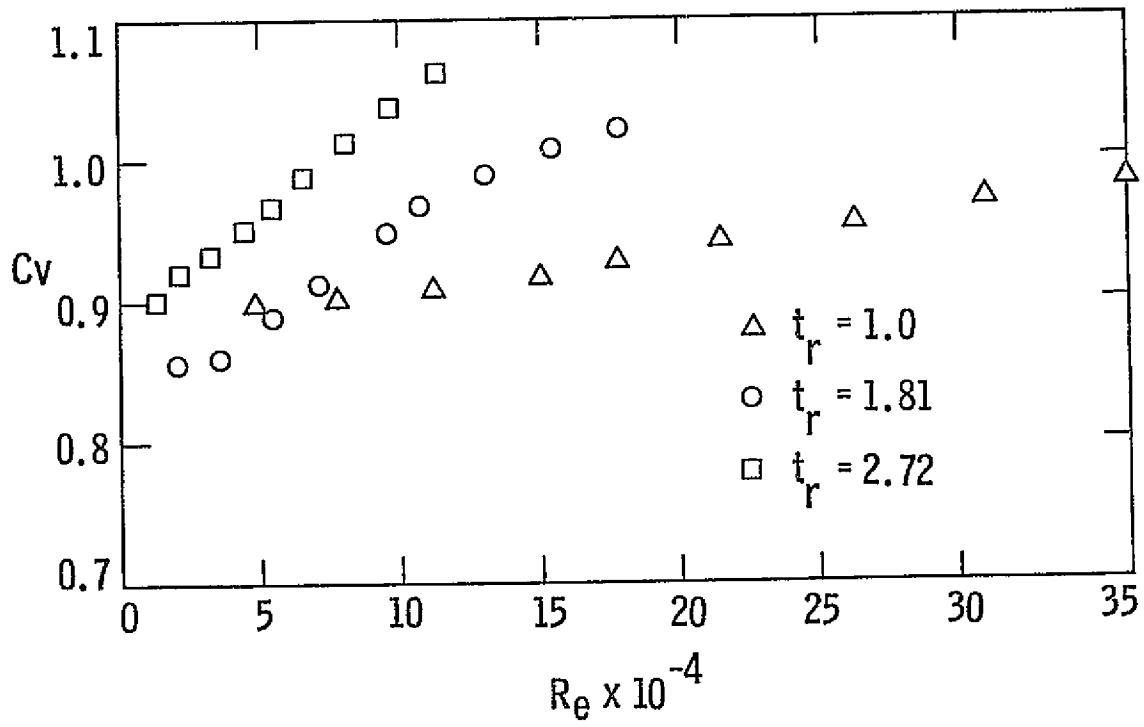

Figure 19. Primary Nozzle Mass Flow Coefficient

changed by externally inducing separation on that wall. The flow then stayed attached to the other wall even after the external disturbance was removed.

The area ratio was reduced to 13.3 while the length of the mixing chamber was maintained at 30.5 cm. Flow separation was not encountered for this area ratio with two leading edge radii of 3.8 cm and 5.1 cm. The thrust augmentation was found to improve by 10 percent as the shroud was moved from 5 cm to 10 cm downstream of the primary nozzle exit.

The geometrical parameters characterizing the configurations tested are given in Table 1. The non-dimensional values were: the area ratio H/d=13.3, the distance from the primary nozzle X/H=1, the mixing chamber length L/H=3, shroud leading edge radius of curvature R/H=0.25, and the ejector aspect ratio S/H=5. The constant area ejector terminates with the mixing chamber. The diffused flow ejector had a 5° half angle straight wall diffuser at the end of the mixing chamber. The diffuser area ratio was 1.30 and its normalized length L'/H=1.75. Tests in the low temperature facility were limited to primary nozzle pressure ratios from 1.06 to 2.0 (M_{ex}=0.3 to choked conditions) at ambient total temperature. In the high temperature facility, the primary nozzle pressure ratio was varied from 1.06 to 3.0. The tests were limited to three values of the total temperature, namely ambient, 255°C, and 540°C. These values correspond to temperature ratios of 1, 1.8, and 2.7 respectively.

3.2 Thrust and Surface Pressure Distribution

The thrust augmentation of both ejector configurations was determined by direct thrust measurements. The results of these measurements in the low temperature facility are presented in figure 20. The ejector thrust normalized with the measured primary nozzle thrust is plotted versus the primary

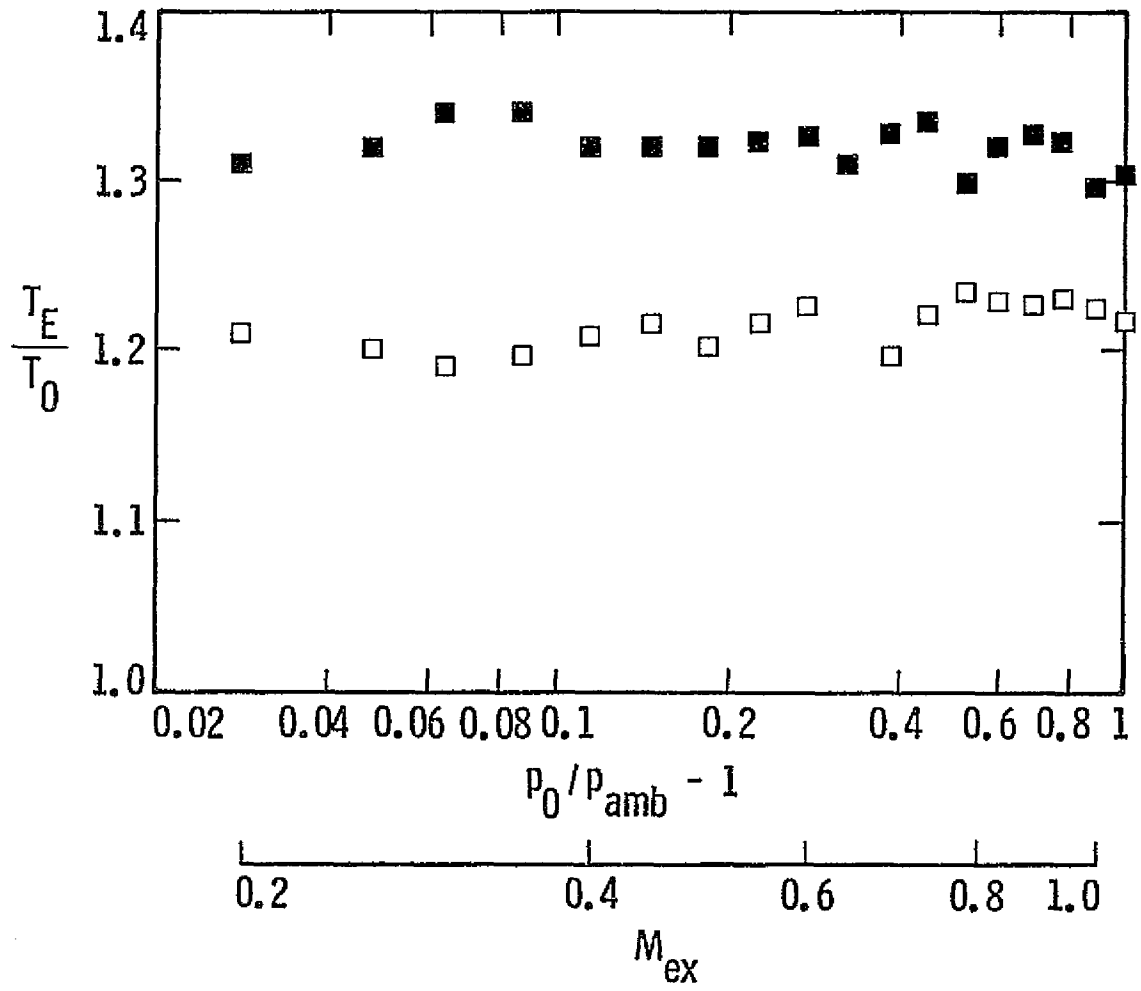

Figure 20. Thrust Augmentation Ratio. Open Symbols Represent Constant Area Ejector. Solid Symbols Represent Diffused Flow Ejector

nozzle pressure ratio. The variation of thrust augmentation ratio with pressure ratio was less than 2.5 percent of the mean. These variations were within the general uncertainty of the measurement technique. Mean thrust augmentation ratio = 1.21 for the constant area ejector and 1.32 for the diffused flow ejector were obtained. These results were obtained for pressure ratios as high as 2. Both ejector configurations were tested up to a pressure ratio of 4.0 in the high temperature facility. These measurements, however, showed a rather large uncertainty ($\mp$ 0.10) for the thrust augmentation ratio, especially at elevated temperatures. Because of this large uncertainty, possible variations of the thrust augmentation with pressure ratio could not be resolved in this phase of the research.

The measured shroud surface pressure distributions are given in figures 21 to 26. Presented in these figures are the results of measurements conducted on both shroud geometries at pressure ratios in the range from 1.06 to 3.0 and at temperature ratios of 1.0, 1.8, and 2.7. The results are plotted in terms of the surface pressure coefficient defined as the pressure differential between the measurement point and the ambient pressure normalized by the dynamic pressure calculated for ideal, one-dimensional, and fully expanded nozzle flow. Under these assumptions, the dynamic pressure is given by the expression

$$q_i = \frac{\gamma}{\gamma - 1} P_{amb} \left[\left(\frac{P_o}{P_{amb}} \right)^{\frac{\gamma - 1}{\gamma}} - 1 \right] \qquad (15)$$

where γ is the ratio of the specific heats. This choice of parameters permits a direct comparison among different pressure distributions in terms of the thrust augmentation since the ideal primary nozzle thrust is proportional to the dynamic pressure.

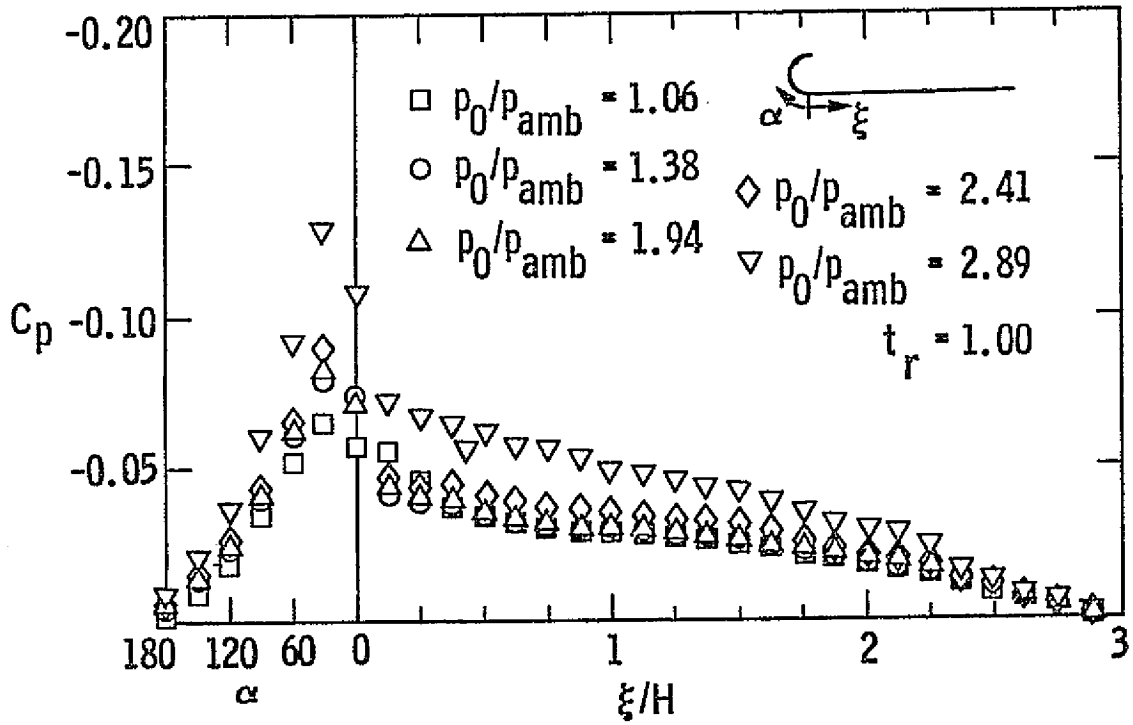

Figure 21. Constant Area Ejector Surface Pressure Distribution at a Temperature Ratio $t_{r=1.00}$

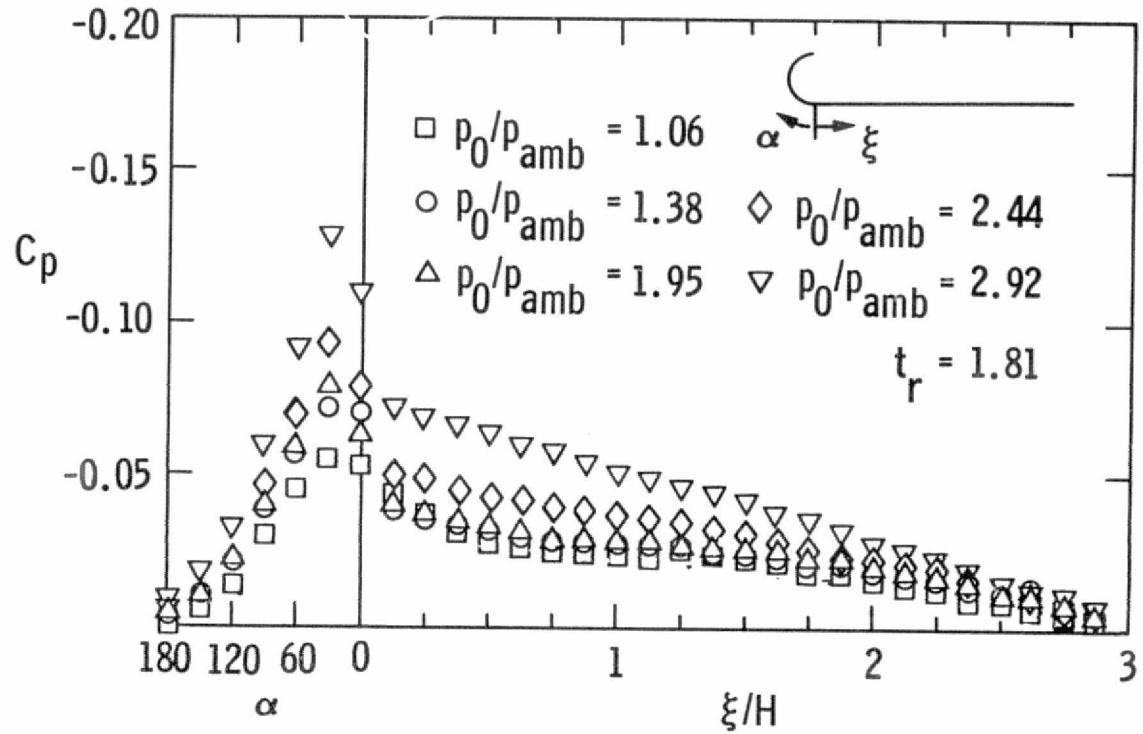

Figure 22. Constant Area Ejector Surface Pressure Distribution at a Temperature Ratio t_r=1.81

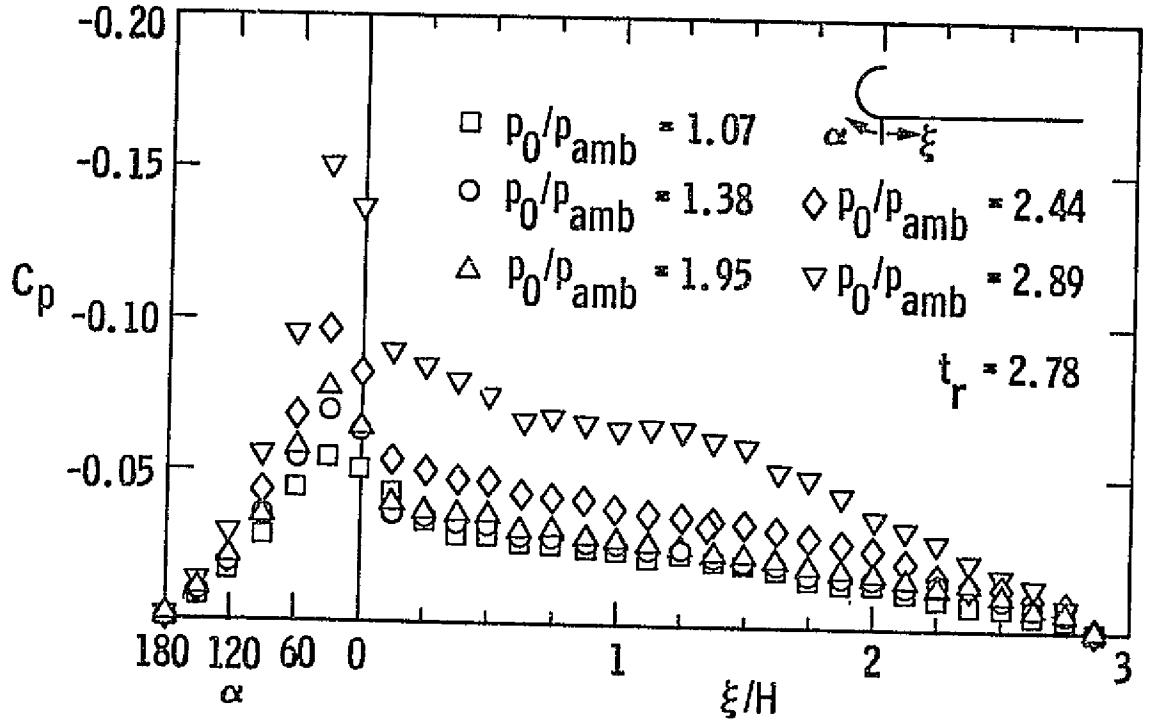

Figure 23. Constant Area Ejector Surface Pressure Distribution at a Temperature Ratio t_r=2.78

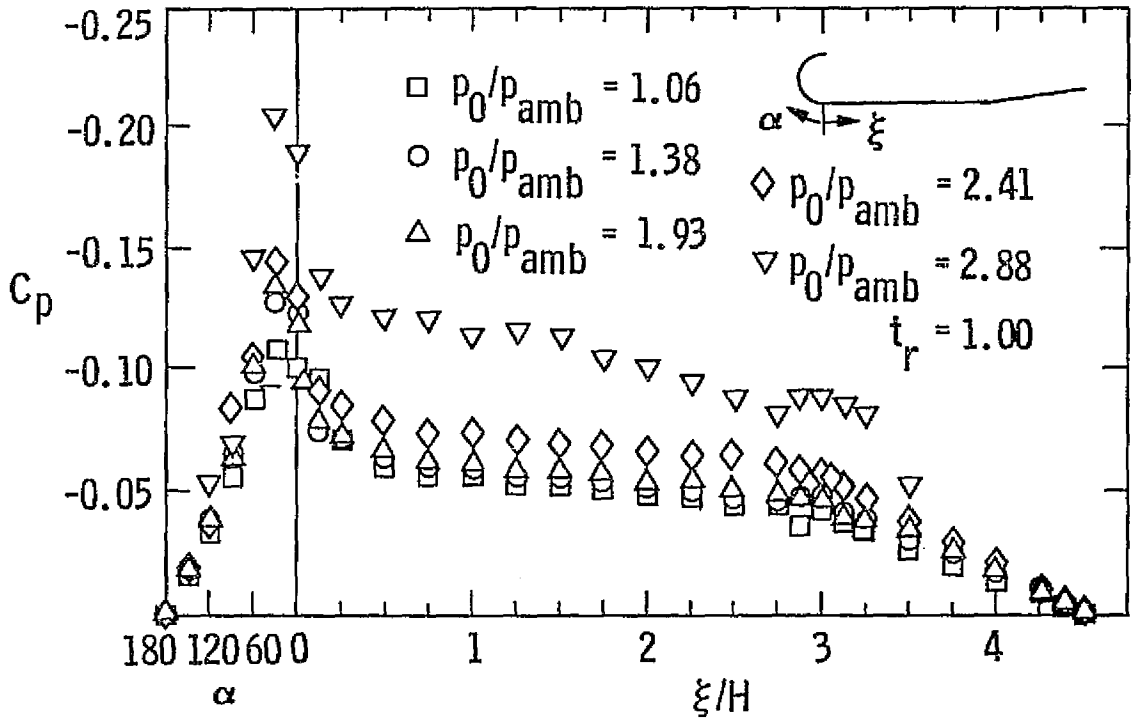

Figure 24. Diffused Flow Ejector Surface Pressure Distribution at a Temperature Ratio t_r=1.00

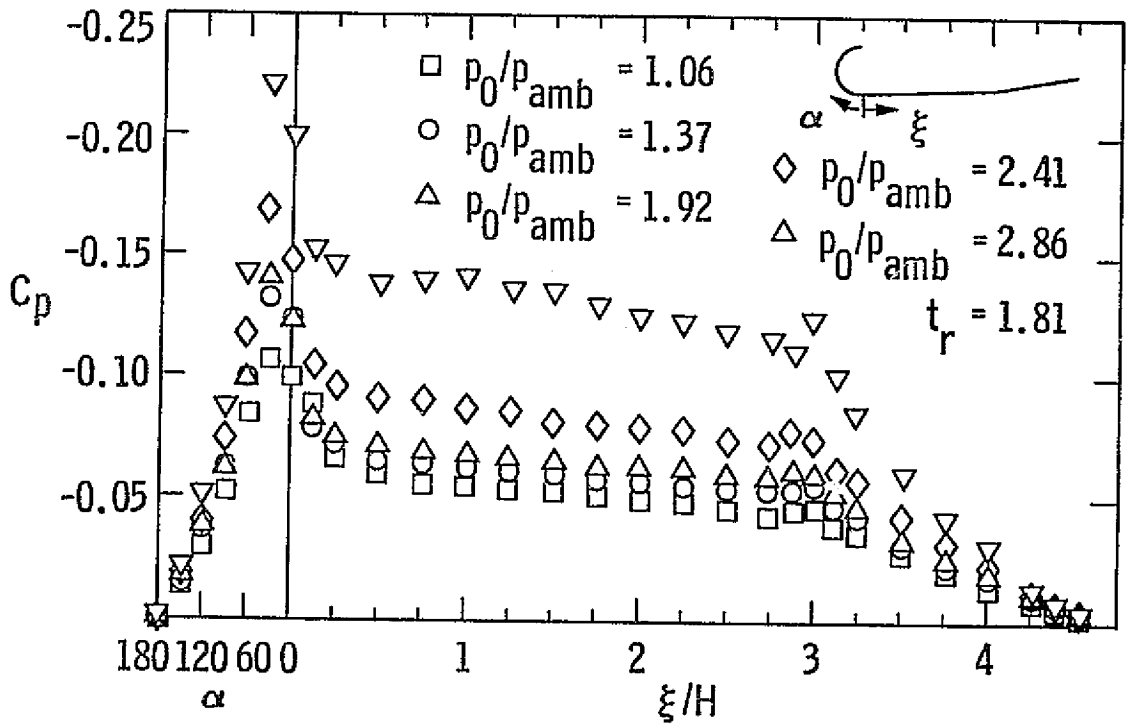

Figure 25. Diffused Flow Ejector Surface Pressure Distribution at a Temperature Ratio t_r=1.81

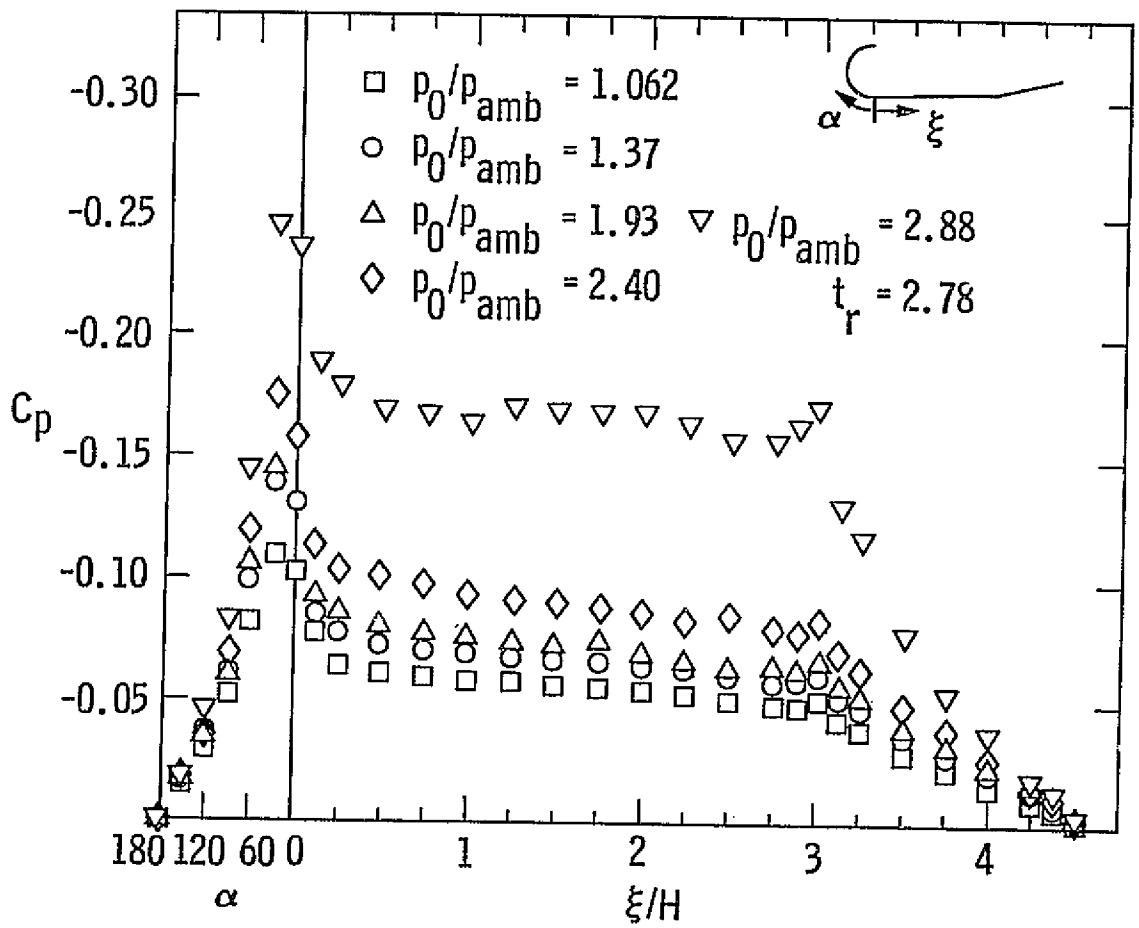

Figure 26. Diffused Flow Ejector Surface Pressure Distribution at a Temperature Ratio t_r=2.78

In comparing the pressure distributions on both configurations, it appears that the significantly lower pressures found in the diffused flow ejector are the result of the pressure recovery along the diffuser. Furthermore, while in the constant area ejector, the pressure recovery is gradual along the mixing chamber; in the diffused flow configuration, the recovery in the mixing chamber is significantly lower. The pressure distribution on the leading edge has a pronounced peak (suction peak). The minimum pressure is located, in all cases, around 30° from the mixing chamber entrance. There is a significant pressure recovery within the first few measurement stations in the mixing chamber. The effect of pressure ratio on the surface pressure coefficient is limited to the leading edge region up to a pressure ratio of 2.0. At higher pressure ratios there is a significant reduction in the surface pressure coefficient throughout the ejector. The effect is particularly pronounced at a pressure ratio of 2.0. The effect of pressure ratio on the leading edge pressure distribution can be characterized by the peak value of the pressure coefficient. These results are presented in figure 27. There is a monotonic decrease of the peak value with the increased pressure ratio. A large change in this peak pressure cofficient was observed at the highest pressure ratio. Temperature ratio does not change the general features of the surface pressure distribution. It does, however, reduce slightly the magnitude of the surface pressure coefficients throughout the shroud wall as the primary flow temperature is increased.

The measured surface pressure was used to calculate the thrust of the system. The results of these calculations are presented in Table 3 where the contribution to the thrust of the shroud surface pressure are normalized by the isentropic thrust of the nozzle, keeping the mass flow rate of the primary nozzle constant. To estimate the thrust augmentation ratio, the following

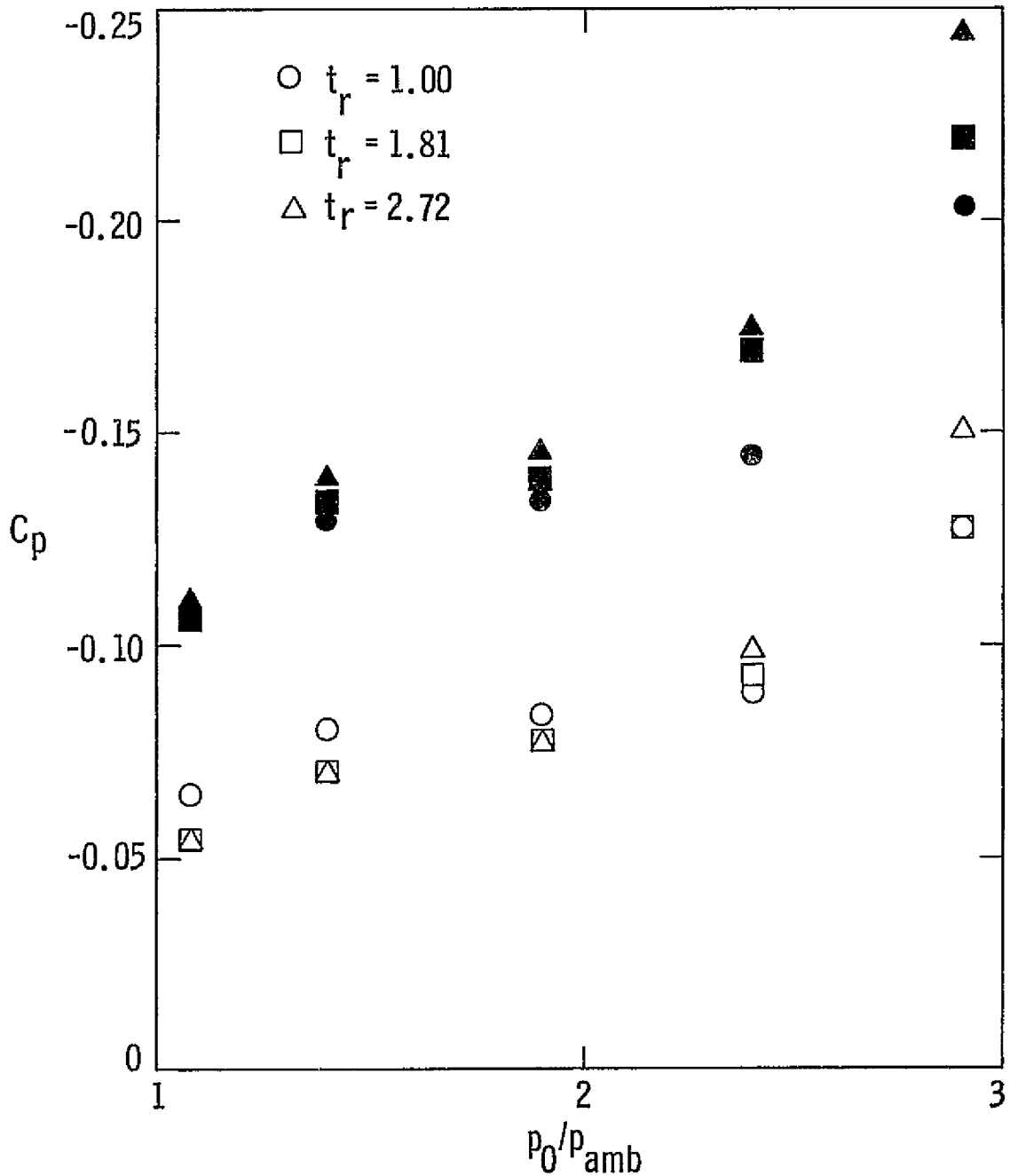

Figure 27. Minimum Surface Pressure Coefficient as a Function of Pressure Ratio. Open Symbols Represent Constant Area Ejector. Solid Symbols Represent Diffused Flow Ejector

assumptions have been made: uniform spanwise distribution of the surface pressure, the forces acting on the external surface of the primary nozzle are negligible, the viscous forces acting on the shroud surface are negligible, and the primary nozzle thrust efficiency equals unity. The overall effect of these assumptions is believed to provide a negative contribution to the system thrust. Thus the values in Table 3 are an upper estimate of the true thrust augmentation ratio.

TABLE 3

Thrust Augmentation Ratio

Surface Pressure Measurements

	Constant Area Ejector			Diffused Flow Ejector		
P_r/t_r	1	1.8	2.8	1	1.8	2.8
1.06	1.24	1.22	1.22	1.40	1.39	1.38
1.38	1.26	1.26	1.24	1.42	1.42	1.41
1.93	1.27	1.26	1.26	1.42	1.42	1.41
2.41	1.29	1.32	1.32	1.44	1.49	1.48
2.88	1.40	1.43	1.45	1.59	1.62	1.57

For the constant area ejector, the above results at low temperature ratios are in agreement with the direct thrust measurements obtained in the low temperature facility (Figure 20). However, the values at a temperature ratio of 2.8 are significantly larger than the values obtained in the thrust measurements. One important effect shown by these results is the significant increase in thrust augmentation ratio at a pressure ratio of 2.88. A significantly increased radiated noise level was observed at this pressure ratio although no quantitative measurements were made. This observation suggests that the aeroacoustic interaction reported by Quinn[32] may be

responsible for the increased thrust augmentation ratio. More work in this area is planned during the phase II effort.

The ejector shroud surface temperature measurements are presented in figures 28 and 29 for the primary flow temperature ratios of 1.8 and 2.7, respectively. The absolute wall temperature normalized with the absolute ambient temperature is plotted as a function of normalized distance along the surface. Little heating of the shroud upstream of $\xi/H=1$ was observed. For the constant area ejector, a gradual rise in surface temperature occurs with the temperature reaching its maximum value at the last measurement point. In the diffused flow ejector a slight decrease in temperature is found in some cases within the diffuser. The effect of increasing pressure ratio is to decrease the temperature at a given location. At a pressure ratio of 2.9 this trend is reversed and large increases in surface temperatures were observed. These results indicate an increased rate of mixing consistent with the observed aeroacoustic interaction in the ejector[33].

3.3 Velocity Field Measurements

The velocity measurements were obtained with the Laser Doppler Velocimeter on both shroud geometries. Two velocity components were measured in the low temperature facility at several pressure ratios. Single component data were taken in the low and high temperature facility as well. These results were obtained at a few pressure ratios and temperature ratios of 1.0 and 1.8.

The centerline velocity results are presented in figure 30 for pressure ratios up to 2 and a temperature ratio $t_r=1$. The downstream component of the mean velocity normalized by the jet exit velocity is plotted versus the downstream distance. Also plotted are the free-jet results. At a fixed pressure ratio and downstream location, the effect of the confining shroud

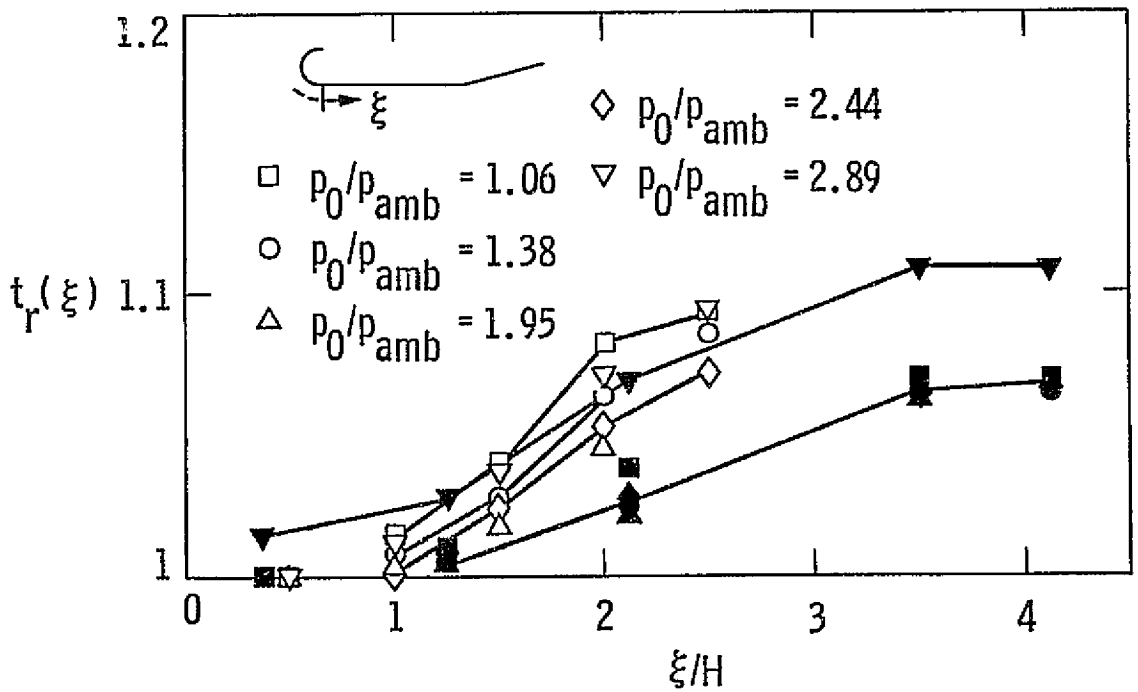

Figure 28. Ejector Shroud Surface Temperature Ratio at a Primary Flow Temperature Ratio t_r=1.81. Open Symbols Represent Constant Area Ejector. Solid Symbols Represent Diffused Flow Ejector

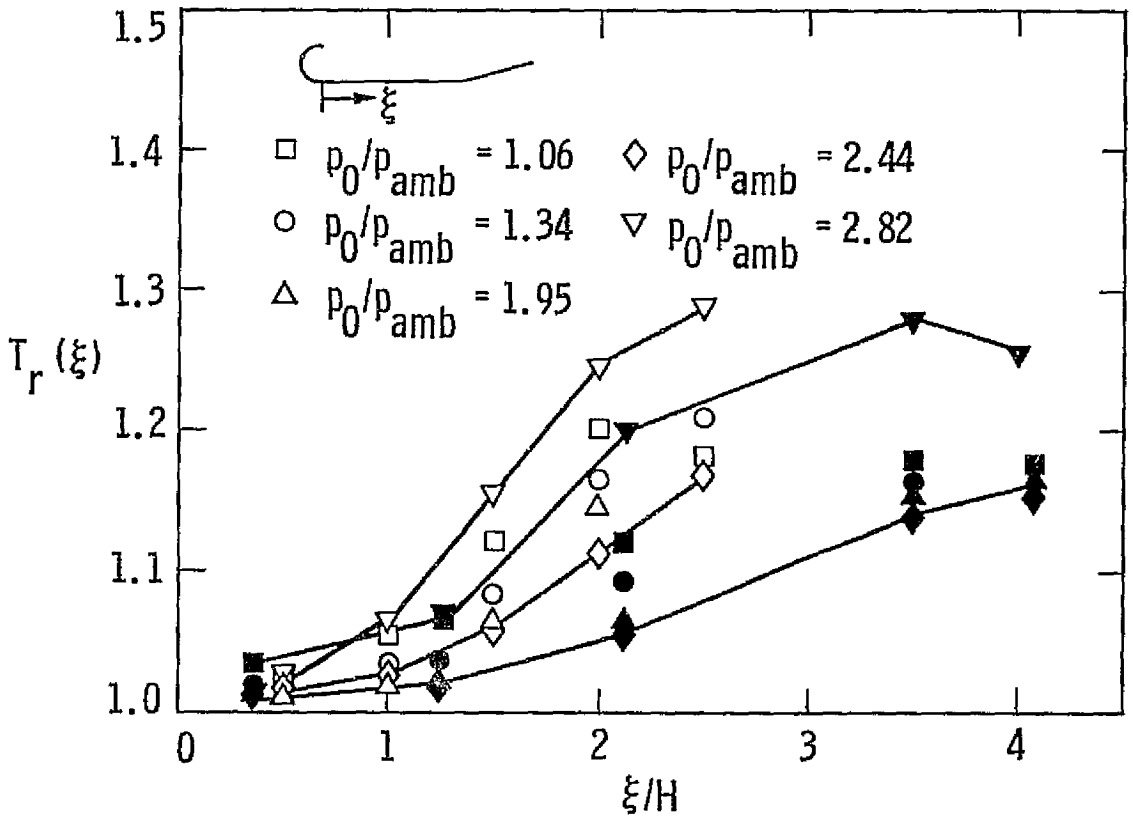

Figure 29. Same as Figure 28 at a Primary Flow Temperature Ratio t_r=2.78

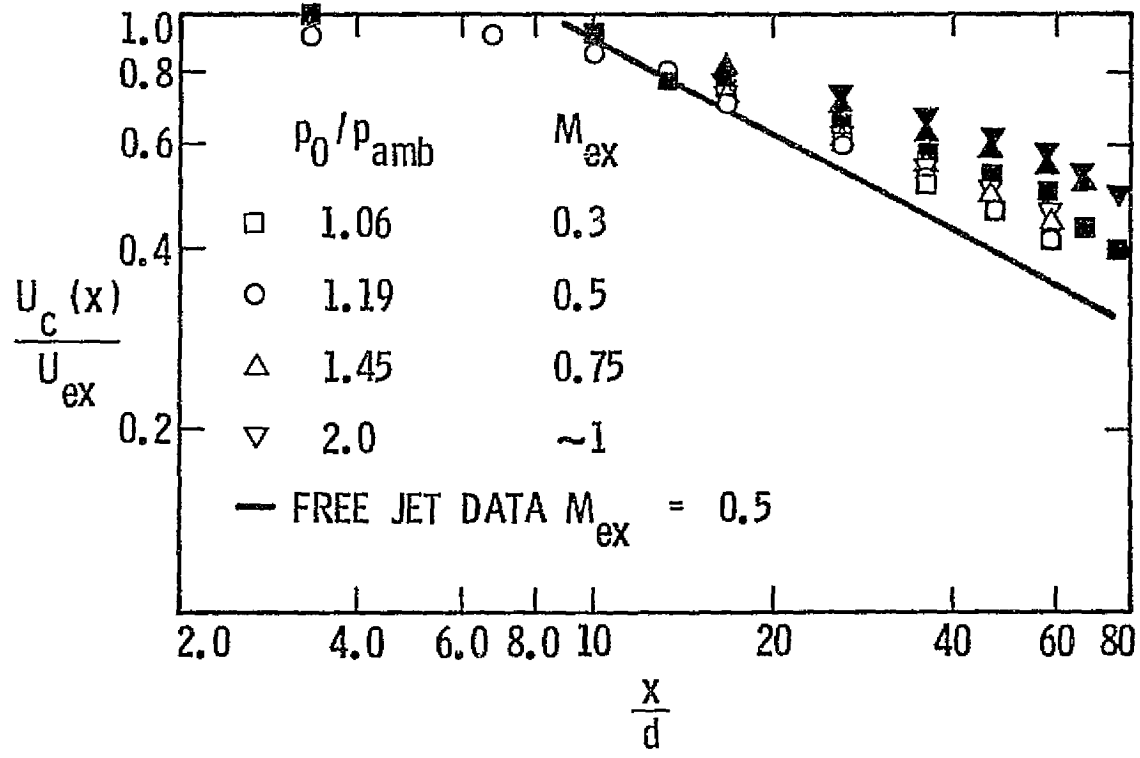

Figure 30. Centerline Velocity Decay. Open Symbols Represent Constant Area Ejector. Solid Symbols Represent Diffused Flow Ejector

surfaces is to increase the normalized centerline velocity. The diffused flow ejector produces a larger increase compared to the constant area ejector. Within the diffuser the centerline velocity decreases at a faster rate than in the mixing chamber. For fixed geometry, an increase in pressure ratio results in an increase in the normalized centerline velocity.

The mean velocity results are presented in figures 31 and 32. The mean velocity normalized with the centerline velocity is plotted versus normalized position. The position across the ejector is normalized with the local width of the ejector. The profiles in the mixing chamber are presented in figure 31 while the profiles in the diffuser are presented in figure 32. For a fixed geometry, possible pressure ratio effects are within the scatter of the measurements. Note that the highest pressure ratio is 2.0. However, the profiles at the entrance of the mixing chamber show significantly larger entrainment for the diffused flow ejector than for the constant area ejector. The downstream evolution of the profiles shows the growth of the primary jet. Downstream of $\xi/H=1.5$ including the diffuser, changes in the mean velocity profiles are small.

The results related to rms value of the fluctuation of U and V components of the velocity and the cross-correlation $\overline{U'V'}$ are presented in figures 33 to 38. These results are presented in the form of profiles of the appropriate quantity normalized with the centerline velocity. The U' velocity profiles are presented in figure 33 for the mixing chamber, and in figure 34 for the diffuser. These results show a minimum at the centerline. This feature is also observed in free-jets[27,28]. The larger than expected scatter of these results obscures possible pressure ratio effects. There is, however, a reduction of the normalized U' values in the diffused flow ejector compared with the constant area ejector. The normalized V' fluctuation

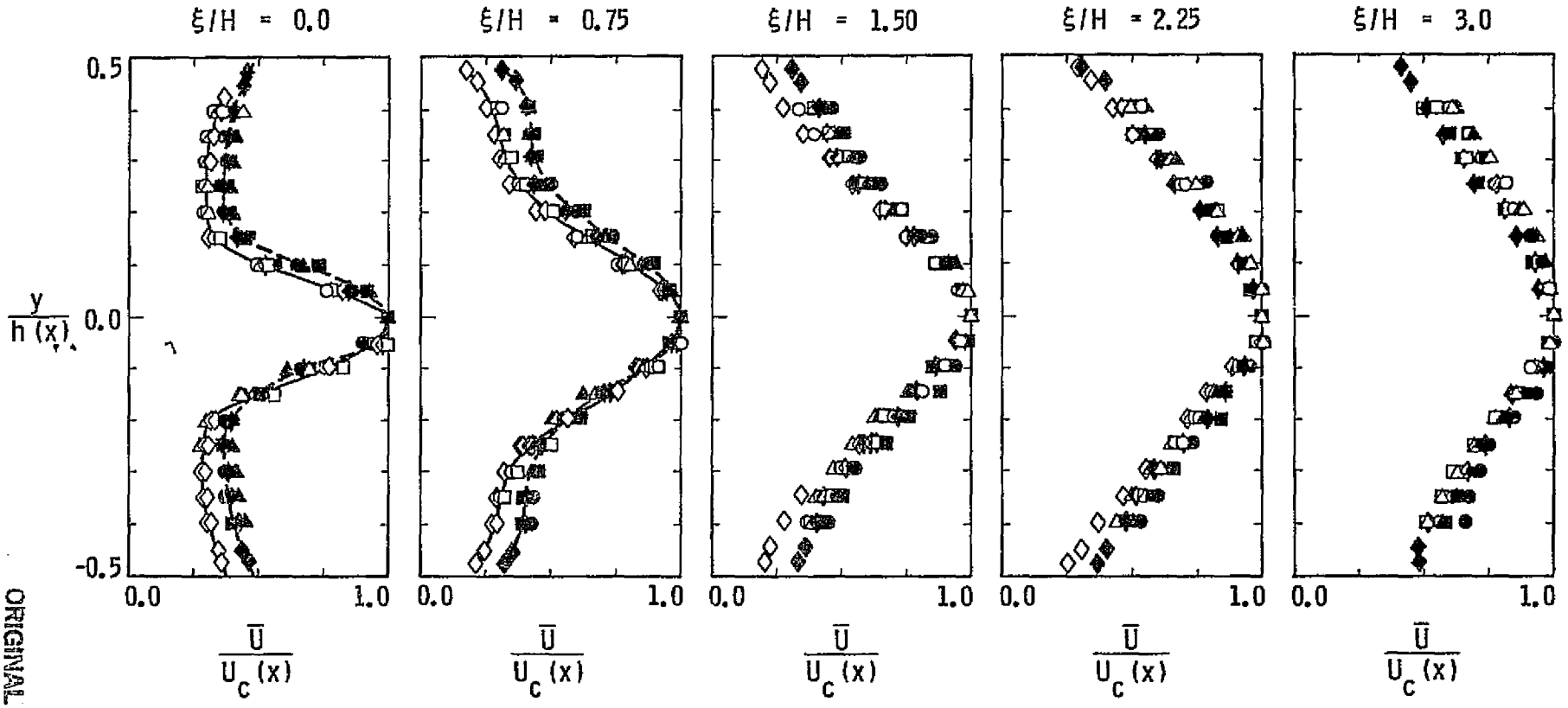

Figure 31. $\bar{U}$ Velocity Profiles in the Mixing Chamber. Open Symbols Represent Constant Area Ejector. Solid Symbols Represent Diffused Flow Ejector. □, P_r=1.06; ○, P_r = 1.45; △, P_r=2.04, ◇, P_r=1.06 one velocity component LDV system

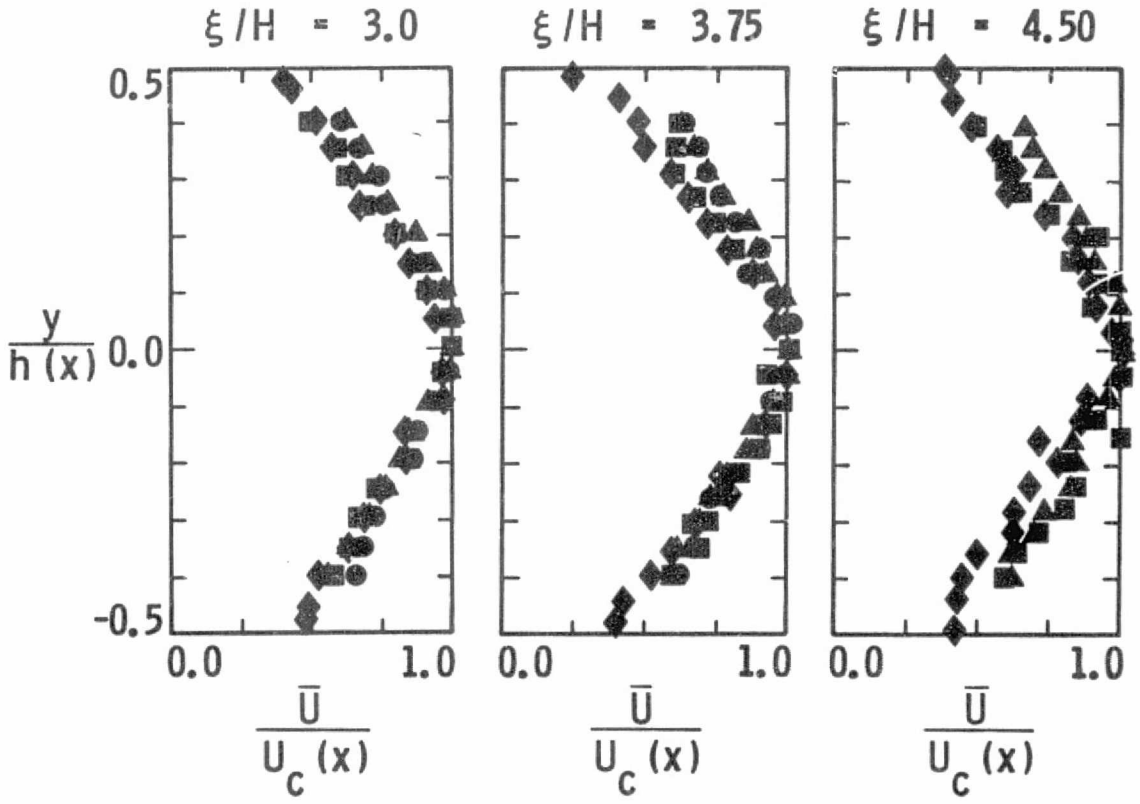

Figure 32. $\bar{U}$ Velocity Profiles in Diffuser. For Key to the Symbols, see Caption, Figure 31

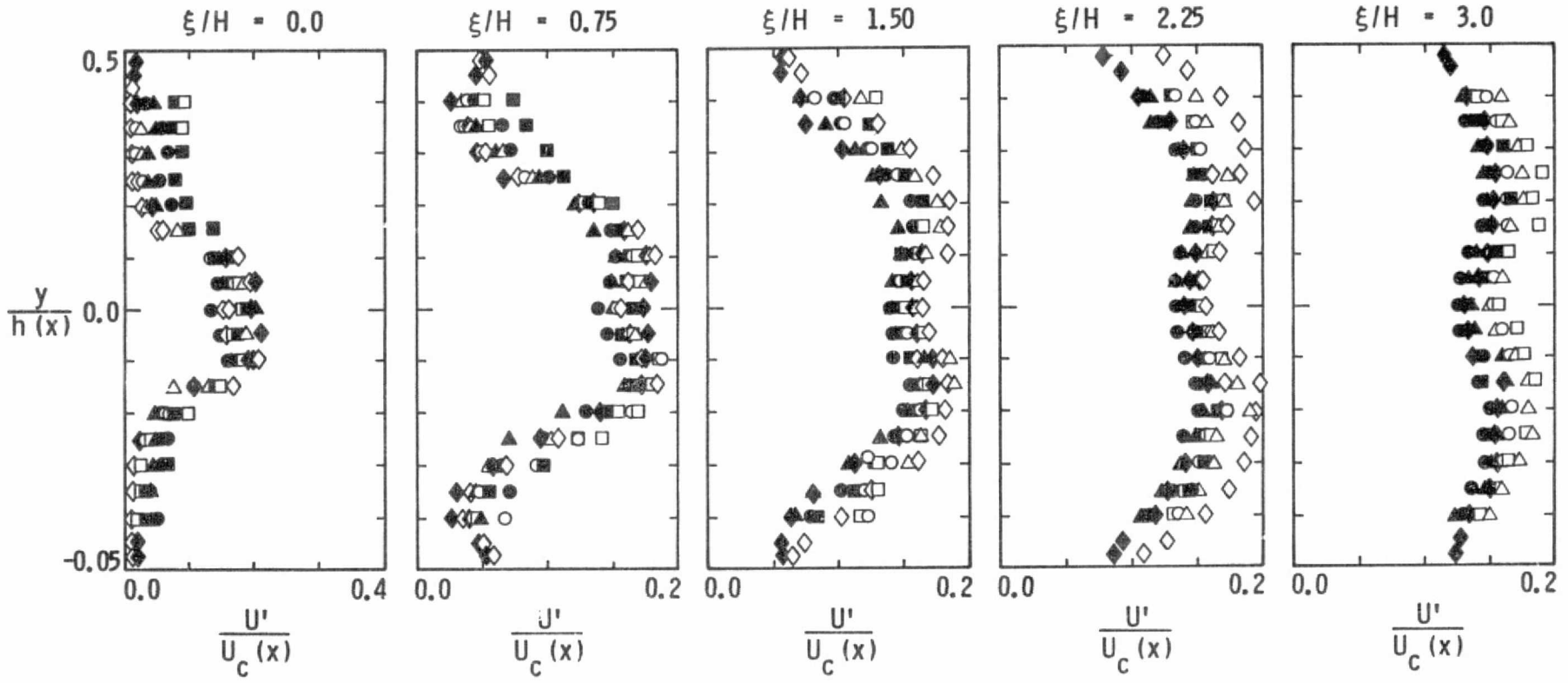

Figure 33. U' Velocity Profiles in Mixing Chamber. For Key to the Symbols, see Caption, Figure 31

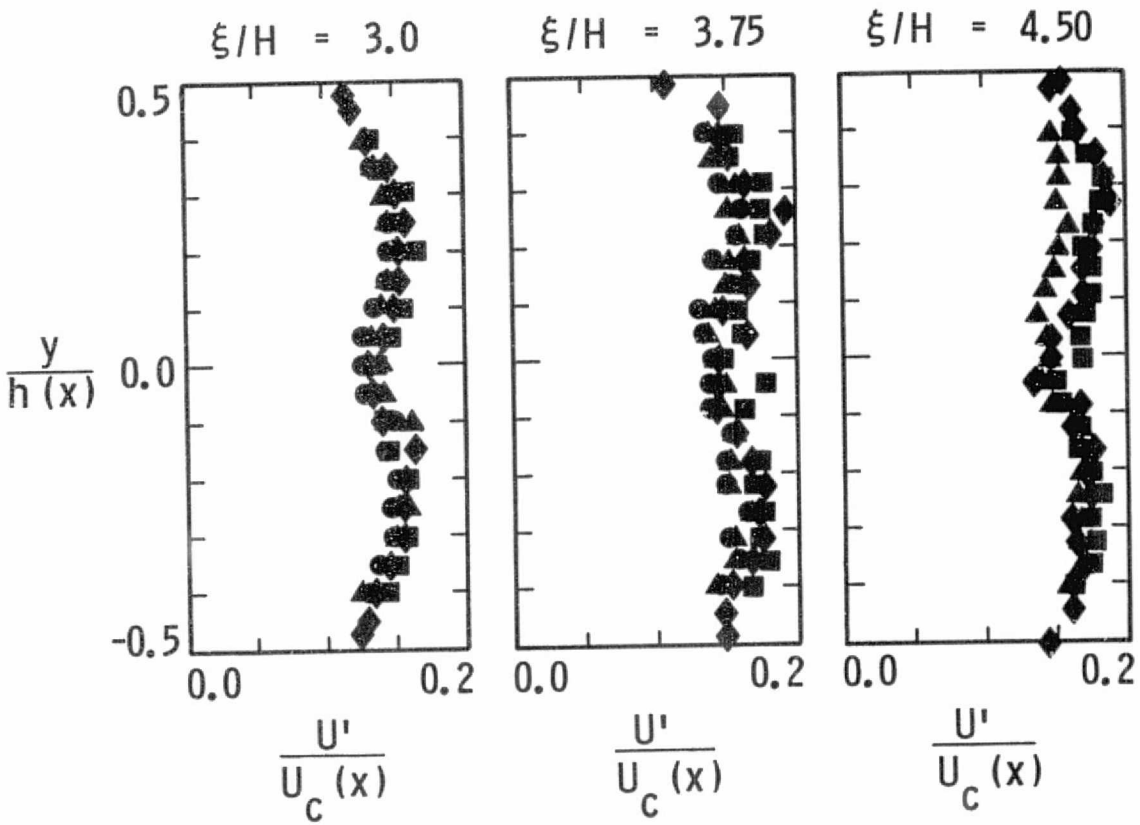

Figure 34. U' Velocity Profiles in Diffuser. For Key to the Symbols, see Caption Figure 31

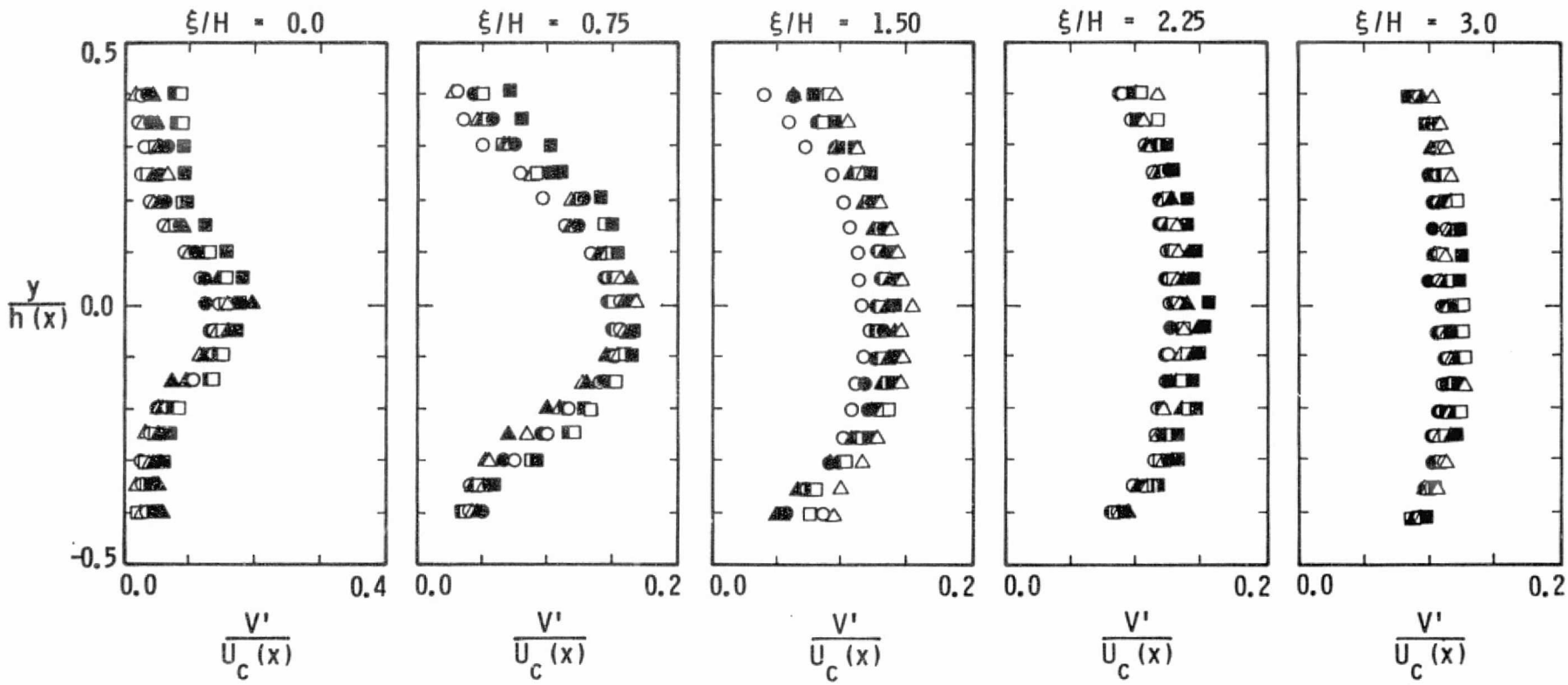

Figure 35. V' Velocity Profiles in Mixing Chamber. For Key to the Symbols, see Caption, Figure 31

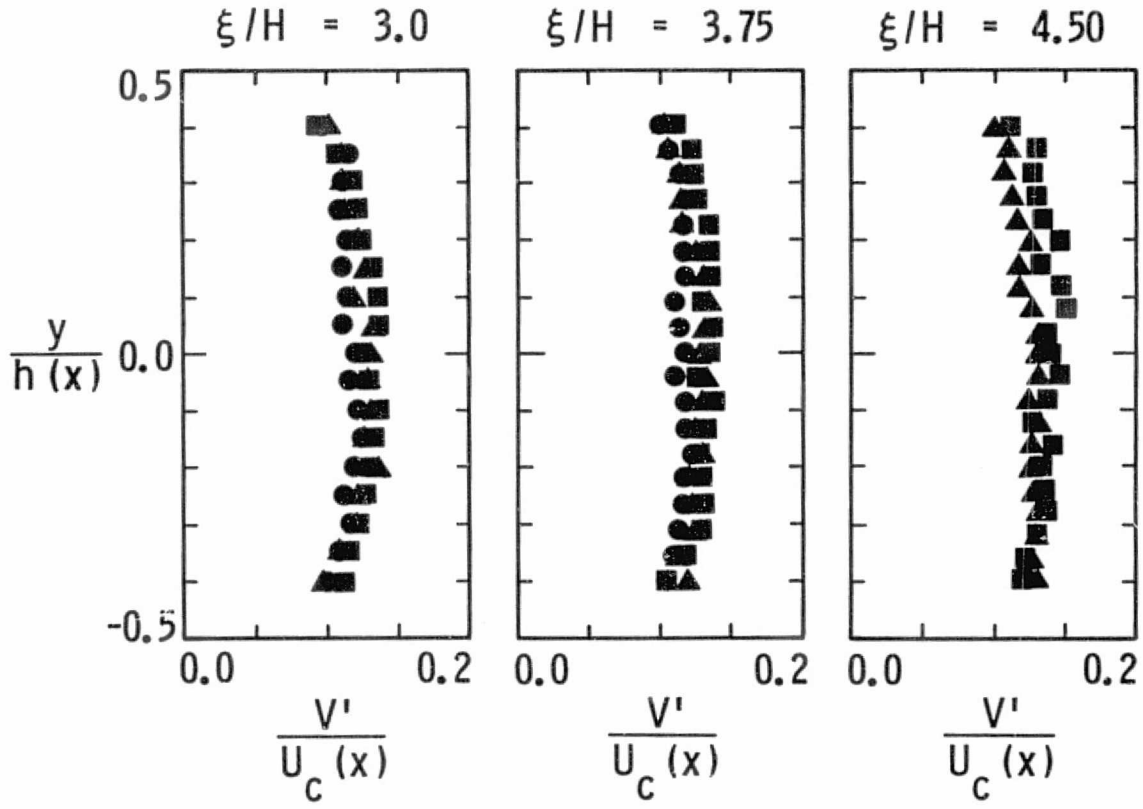

Figure 36. V' Velocity Profiles in Diffuser. For Key to the Symbols, see Caption, Figure 31

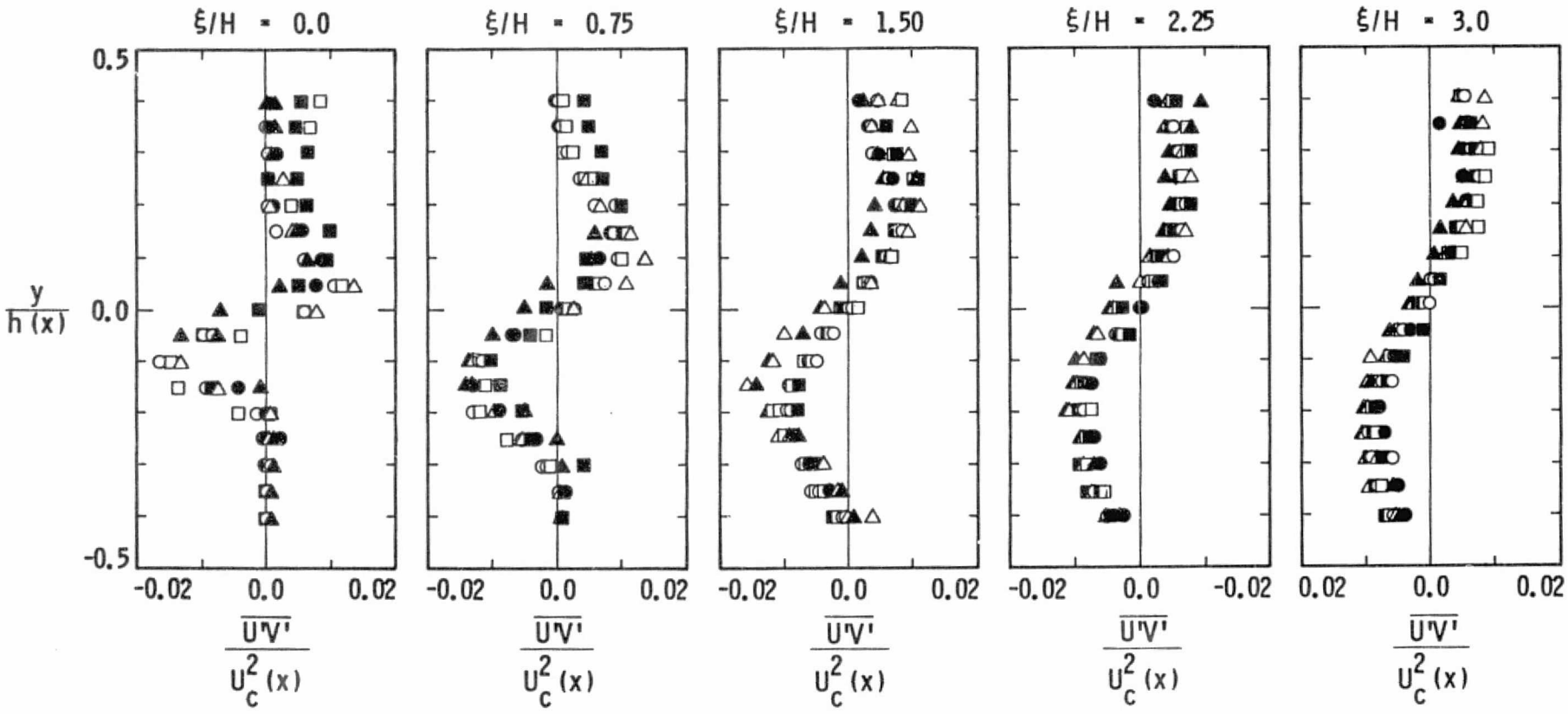

Figure 37. $\overline{U'V'}$ Correlation Profiles in the Mixing Chamber. For Key to the Symbols see Caption, Figure 31

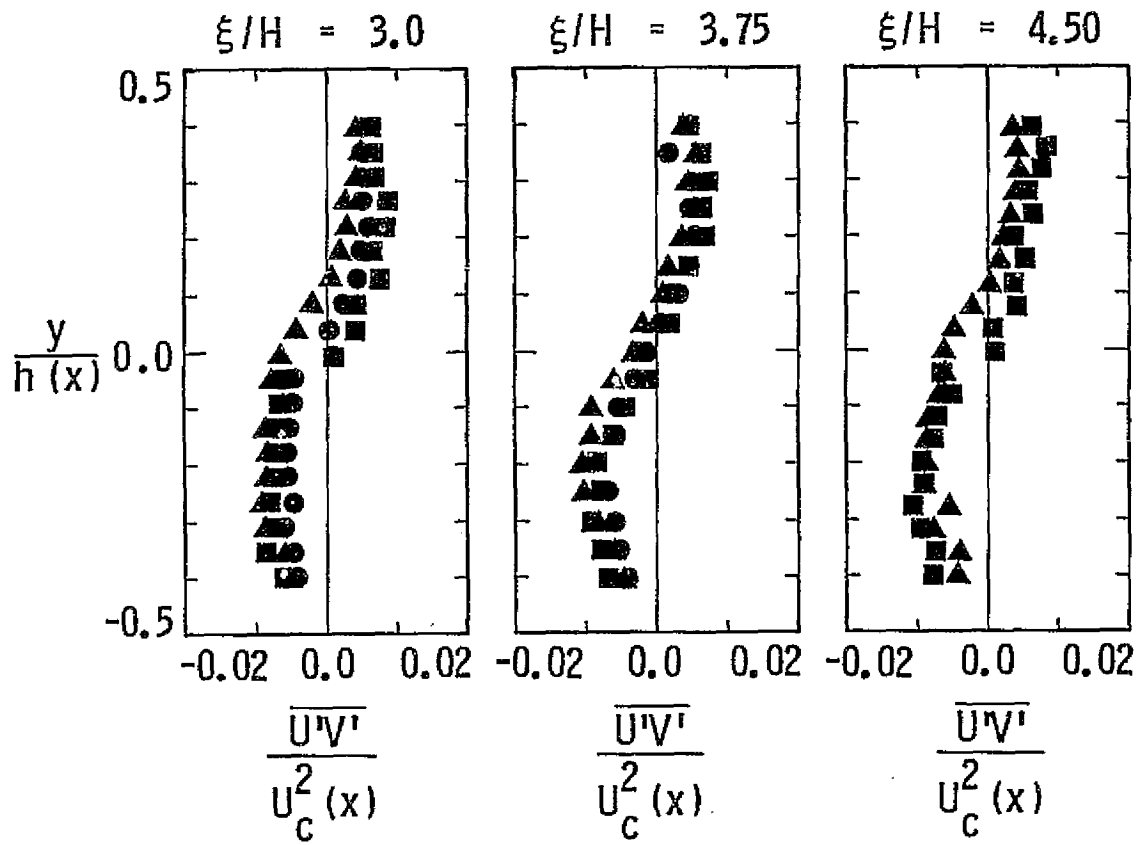

Figure 38. $\overline{U'V'}$ Correlation Profiles in the Diffuser. For Key to the Symbols see Caption, Figure 31

profiles are shown in figures 35 and 36. These measurements did not show a local minimum of V' on the centerline. There are some contradicting results as to whether or not there is such a minimum in a free jet[28,29]. The normalized $\overline{U'V'}$ velocity profiles are shown in figures 37 and 38. Within the scatter of the measurement, the normalized values of U', V' and $\overline{U'V'}$ are independent of pressure ratio. Comparison between the results obtained in the constant area ejector and diffused flow ejector shows no significant differences except for the above mentioned effect on the U' measurements. The downstream evolution of the first order correlations presented above showed the jet surrounded by the low turbulence induced flow at the entrance of the mixing chamber. As the flow develops further downstream, significant turbulent transport is found near the shroud. Downstream of $\xi/H=1.5$ the turbulent correlation profiles do not change significantly, even within the diffuser.

The mean velocity results obtained in the high temperature facility are presented in figures 39-41. The centerline velocity decay is presented in figure 39. At a temperature ratio $t_r=1$ the results are in good agreement with those obtained in the low temperature facility (figure 30). At temperature ratio $t_r=1.8$, significantly lower values of the normalized centerline velocity were found. The downstream evolution at $t_r=1.8$ is very similar to that found at $t_r=1.0$. The mean velocity profiles are presented in figures 40 and 41 for primary nozzle pressure ratios of 1.06 and 1.39 respectively. Results on both configurations at temperature ratios $t_r=1.00$ and 1.8 are presented. These measurements had considerable scatter. The results obtained at a temperature ratio $t_r=1$ are in reasonable agreement with the results obtained in the low temperature facility. Within the scatter of the measurement, the results at a temperature ratio $t_r=1.8$ indicate no significant effect of temperature ratio on the mean velocity profiles.

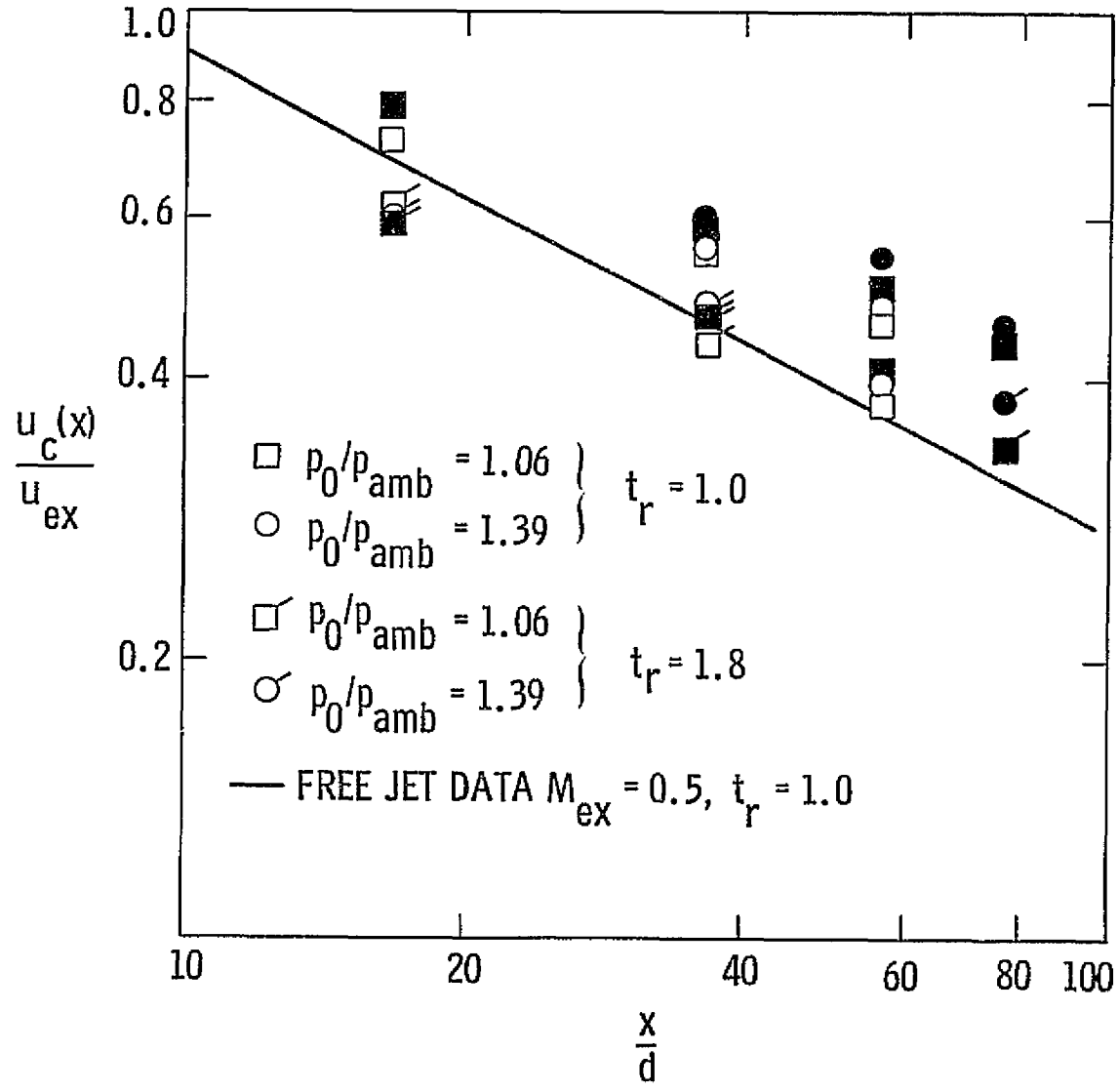

Figure 39. Centerline Velocity Decay. High Temperature Facility Results. Open Symbols Represent Constant Area Ejector. Solid Symbols Represent Diffused Flow Ejector

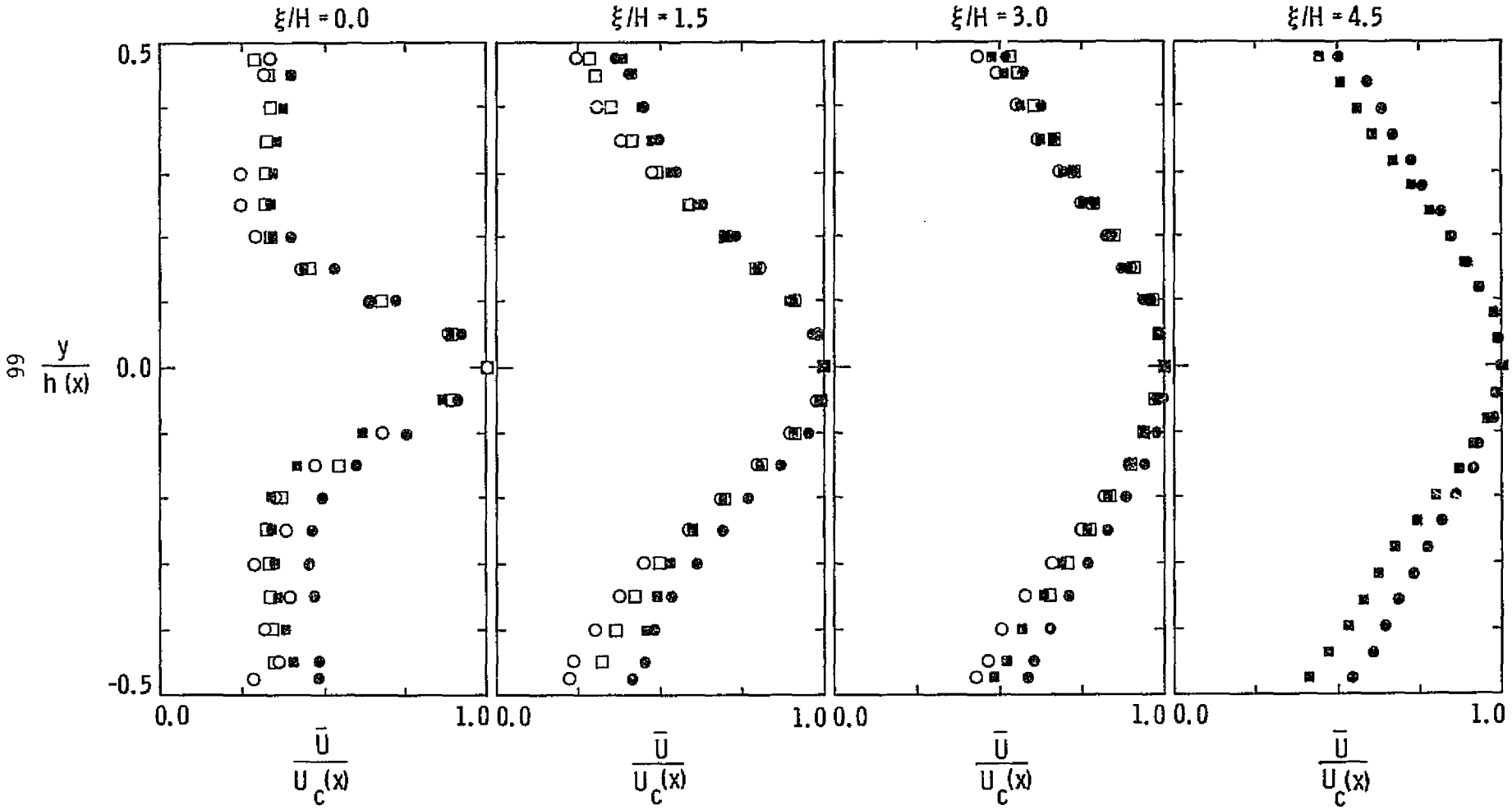

Figure 40. Normalized Mean Velocity Profiles. High Temperature Facility Results at a Pressure Ratio P_o/P_{amb}=1.06 and □ t_r=1.0, o t_r=1.8. Open Symbols Represent Constant Area Ejector. Solid Symbols Represent Diffused Flow Ejector

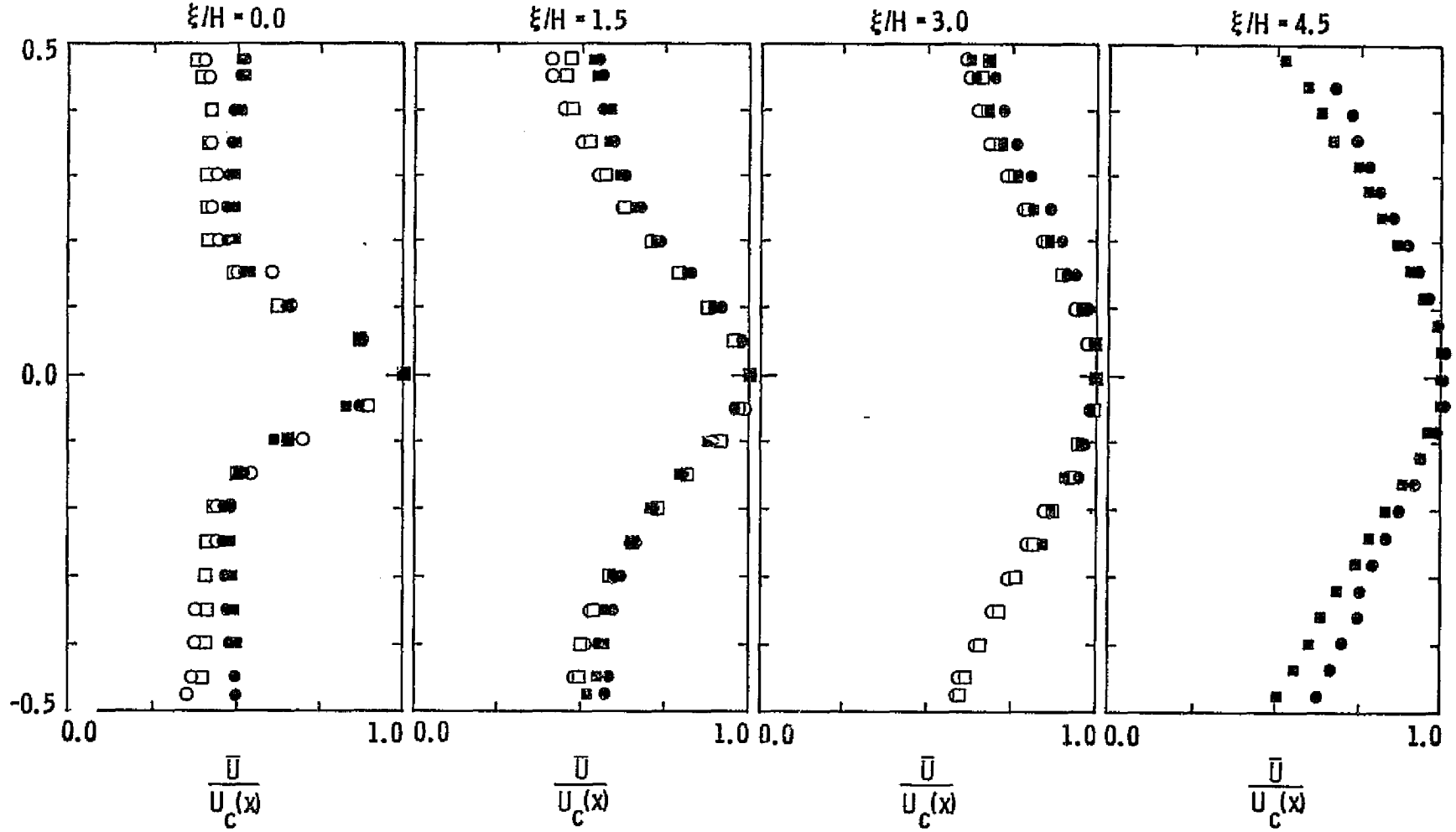

Figure 41. Normalized Mean Velocity Profiles. High Temperature Facility Results at a Pressure Ratio P_o/P_{amb}=1.39. For Key to Symbols see Caption, Figure 40

3.4 Entrainment and Mixing Results

The measured velocity profiles were used to calculate the mass flow rate per unit span through the ejector. The assumption was made that the density is constant across the flow, its value equal to the ambient value. This calculation provides a test of the accuracy of the measurements since the mass flow rate through the ejector should be constant. The variations of the calculated mass flow rate with downstream distance were always less than 2 percent of the mean. The calculated mass flow rate normalized with the isentropic mass flow rate of the primary nozzle is presented in Table 4. In both configurations, the normalized mass flow decreases with pressure ratio. The diffused flow ejector has a higher mass flow rate. The difference varies from 17 percent at low pressure ratios to 27 percent at a pressure ratio of 2.0.

TABLE 4

Entrainment Ratio

P_o/P_{amb}	Constant Area	Diffused Flow
1.06	4.56	5.36
1.19	4.15	----*
1.45	4.16	5.39
2.00	3.87	4.93

The effect of mixing on the downstream evolution of the mean velocity is shown in Figure 42. In this figure, the velocity at three points in the profile normalized with the volume rate average velocity, <U>, is plotted as a function of downstream distance. At the entrance of the shroud, the velocities at y/h=0.0 and 0.4 decrease while at y/h=0.2 the velocity increases as a function of downstream distance. For ξ/H=0.75 to 1.5 the trend is reversed

* Incomplete LDV data taken for entrainment calculations

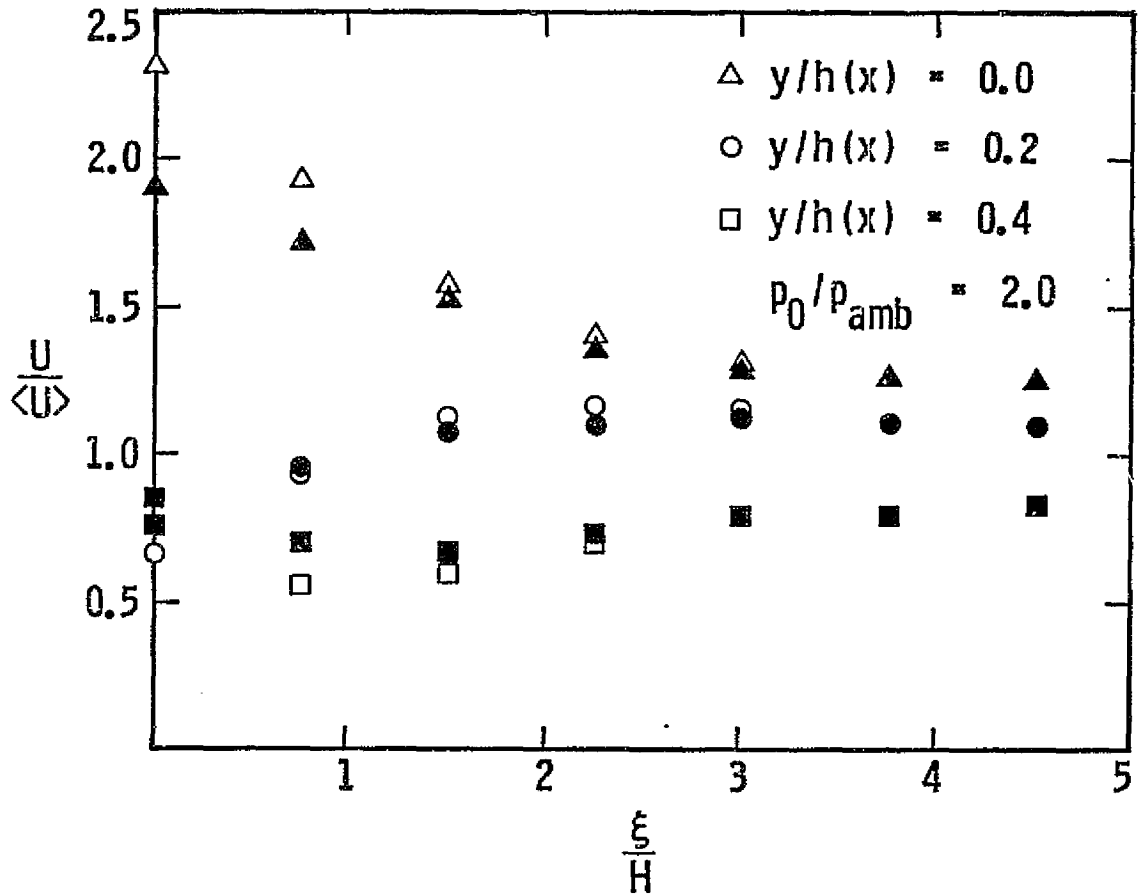

Figure 42. Downstream Evolution of the Mean Velocity in the Ejector. Open Symbols Represent Constant Area Ejector. Solid Symbols Represent Diffused Flow Ejector

near the shroud surface. At the downstream end of the mixing section and in the diffuser ($\xi/H>1.5$), no significant changes occur although the values are different across the flow. Effects of shroud geometry on this evolution were small and more pronounced at the entrance of the ejector. Similar results were obtained at other pressure ratios.

The nonuniformity of the mean velocity profiles can be characterized by the parameter λ, defined by the relation[9]:

$$\lambda = \frac{h(x) \int U^2(x)dy}{(\int Udy)^2} \qquad (16)$$

This parameter was calculated by integration of the velocity profiles over the measured portion of the cross section. The results for a pressure ratio of 2.0 are presented in Table 5. As discussed earlier, the normalized velocity profiles do not depend on pressure ratio. Therefore, neither should λ. The effect of shroud geometry on λ is limited to the shroud entrance region ($\xi/H<1.5$) where a significantly lower value is found in the diffused flow configuration. At the downstream end of the mixing chamber and throughout the diffuser, the values of λ are indicative of a well mixed profile. Also significant is the little variation in the value λ observed within the diffuser ($\xi/H>3.0$).

TABLE 5

Mixing Parameter λ at $P_o/P_{amb}=2.0$

ξ/H	Constant Area	Diffused Flow
0.00	1.28	1.15
0.75	1.20	1.12
1.50	1.09	1.08
2.25	1.05	1.04
3.00	1.03	1.03
3.75	----*	1.03
4.50	----*	1.02

*Insufficient LDV data taken for entrainment calculations

IV. DISCUSSION

(i) Interacting Regions

The test conducted with the constant area ejector of area ratio 16.7 did not show significant thrust augmentation. The flow visualization results suggest that the primary jet failed to interact with the shroud wall. The small area ratio results showed significant thrust augmentation and as the turbulent correlation measurements indicate, the interaction between the primary jet and the shroud did occur. This aspect of the flow can be readily understood by considering the non-interacting case shown in figure 43. A fluid element following the trajectory A-B must have a total pressure equal to the ambient pressure. Because the fluid element does not enter the turbulent region, its total pressure remains constant. As the fluid element reaches point B the static pressure becomes atmospheric and, therefore, fluid velocity vanishes, i.e., incipient separation. We see then that for the ejector to provide significant thrust augmentation, turbulent momentum transfer must occur throughout the entire cross section at least in some portion of the ejector. Because this momentum transport is characterized by non-zero $\overline{U'V'}$ velocity correlations, an estimate can be made of the minimum value of the ratio L/H in order to achieve significant thrust augmentation. We use for this estimate the well established free-jet results. The results of Gutmark and Wygnanski[29] show very small $\overline{U'V'}$ velocity correlations at $y/x \approx 0.2$; thus, by taking $H=2y$ and $L=x$, we find $L_m/H=2.5$, where L_m is the minimum length below which no significant thrust augumentation is observed. The value of this parameter for the large area ratio configuration is $L_m/H=2.67$, and agrees with our estimate. It should be pointed out that the use of self-similar free-jet results is justified only in large area ratio ejectors for which the interaction occurs sufficiently far downstream.

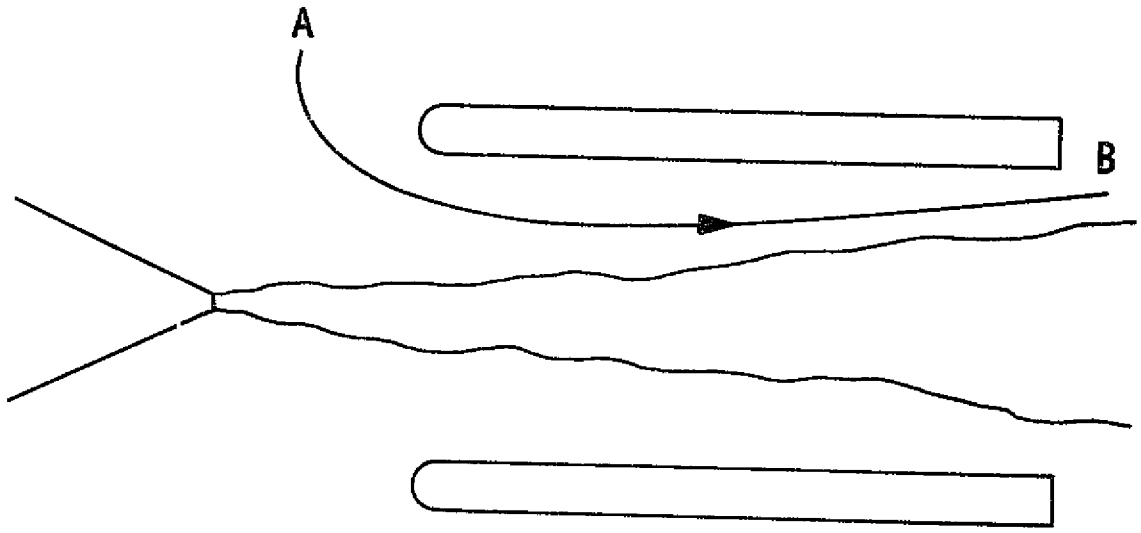

Figure 43. Non-Interacting Ejector Flow

(ii) Flow Regions

The lateral momentum transport is related to the $\overline{U'V'}$ velocity correlations presented in Figures 37 and 38. While at the entrance of the ejector, turbulent transport is limited to the center of the shroud; further downstream there are non-zero $\overline{U'V'}$ throughout the entire cross section. The $\overline{U'V'}$ velocity profiles (figures 37 and 38) also show the existance of two regions. At the centerline, a positive derivative of $\overline{U'V'}$ with respect to y indicates a reduction of momentum with downstream distance as shown in figure 42. Away from the centerline, near the shroud surface, the derivative of $\overline{U'V'}$ with respect to y is negative, which produces a positive contribution to the downstream momentum. An increase of momentum with downstream distance near the shroud is evident in the results presented in figure 42. As the flow develops downstream, the position of the maximum $\overline{U'V'}$ moves outwards, presumably until it reaches the shroud. At this point the second region terminates and no further increase of momentum can be obtained. Therefore, a critical length L_c of the ejector can be defined as the length of the shroud for which the maximum $\overline{U'V'}$ first reaches the wall. This critical length can readily be identified as the borderline between the short and the long ejectors[33]. Using again the well established free-jet results, an engineering estimate of this critical length can be obtained. For both two-dimensional and axisymmetric free jets, the maximum $\overline{U'V'}$ occurs at y/x=0.08. From this value it is found $L_c/H=6.25$ where H is the width or diameter of the mixing duct in two-dimensional or axisymmetric configurations respectively. This result is validated by the measurements of Quinn[34] in axisymmetric configurations and at low pressure ratios. The above estimates apply primarily to constant area ejectors which do not have adverse pressure gradient. The effect of diffusion will result in an increase in the value of L_m and L_c. A proper value of the width H should be used to characterize not

so much the width of the shroud but rather it should characterize the distance across the flow between primary nozzle elements (multinozzle) and/or the wall.

In considering the role of mixing in ejector performance, the parameters L_m and L_c introduced above can also be employed to define three distinctive ejector regions. The entrance region, $x<L_m$, is characterized by the lack of direct interaction between the shroud wall and the primary jet. This region covers the leading edge of the shroud and a portion of the mixing chamber. The interaction region, $L_m<x<L_c$, is characterized by the positive interaction between the primary jet and the shroud wall. This interaction results in positive pressure and momentum gradients near the wall. Finally, the "pipe" flow region, $L_c<x$, is characterized by a negative interaction of the turbulence with the wall: negative in the sense that it causes an increase of skin friction without a significant improvement in the uniformity of the velocity profiles. Because the lengths of the ejectors tested in this investigation are shorter than L_c, this third region could not be documented. There is, however, considerable evidence of its existence[34].

(iii) Flow Structure - Constant Area

The ejector geometries investigated in this program have length-to-width ratios of 4.25 and 6 for the constant area and the diffused flow ejectors respectively. They are, therefore, short ejectors from the point of view of mixing development. The velocity field measurements show significant changes as compared to free-jet values. The centerline velocity decay (figure 30) is significantly reduced by the confining shroud. The reduced jet growth is the result of the coflowing induced flow[35]. The adverse pressure gradient inside the mixing chamber may increase the jet growth rate. However, it appears that the effect of the coflowing stream dominates over the adverse

pressure gradient. Peak values of the turbulent correlations normalized with the centerline velocity are 25 percent lower than those found in two-dimensional free jets[28,29]. However, if the measured profiles at $\xi/H=0.0$ are normalized with the velocity difference between the jet and the coflowing stream, the results are in good agreement with free-jet values. This suggests that the underlying turbulent structure in the jet with coflowing stream is similar to that found in free jets. The effects of pressure ratio (up to $P_o/P_{amb}=2$) on the velocity field are small. The effect of temperature ratio is significant in the centerline velocity decay. The observed reduction of the centerline velocity can be the result of rapid cooling of the gas. The increased density associated with the flow cooling will result in a velocity reduction.

(iv) Flow Structure - Diffuser

The effect of diffusion on the velocity field can be determined by comparison of the results obtained in the two geometries. As expected, the effect of diffusion is to increase the entrainment ratio of the ejector for the same ejector width. The mean velocity profiles (figure 31) show that while in the entrance region, the increase is primarily the result of an increase of the coflowing velocity; in the interaction region, the increase is primarily in the centerline velocity and the profiles remain similar in both geometries. The evolution of the uniformity of the velocity is also different in both geometries. The diffused flow ejector shows a significantly lower value of the parameter λ at the entrance. At the end of the mixing chamber the same value of λ is found in both geometries, indicating a slower rate of mixing in the diffused flow ejector configuration.

(v) Surface Pressure Measurements

The existance of these regions in the ejector is also shown by the shroud surface temperature measurements (figures 28 and 29). In the entrance region the surface temperature is essentially ambient. A slight increase in temperature is the result of heat transfer by radiation and conduction through the wall. In the interaction region the turbulent transport results in a gradual increase in the surface temperature. The effect of pressure ratio is to reduce the wall temperature as the pressure ratio is increased, indicating reduced turbulent transport. Only at a pressure ratio of 2.9 is a significant increase in surface temperature found. This result is consistent with the increase in mixing proposed by Quinn[34] as a result of the aeroacoustic interaction. The surface temperatures in the constant area ejector reach higher values than in the diffused flow ejector. Furthermore, the highest temperature is reached in a shorter distance in the constant area configuration. This result is consistent with the entrainment and mixing results presented above. The constant area ejector has a larger rate of mixing and reduced entrainment ratio, both factors contributing positively to an increase of the surface temperature. Of course, this argument applies to the results obtained at a pressure ratio less than 2.9.

The surface pressure measurements show a pronounced peak (suction peak) on the leading edge (figures 21 to 26). The general features of this peak and the mean velocity results at the entrance of the mixing section (figure 31) are reminiscent of airfoil leading edge behavior. The transition to the interaction region is not apparent from the surface pressure measurements. Outside the leading edge suction peak, pressure recovery in the diffused flow ejector is primarily achieved in the diffuser. The recovery in the mixing chamber is quite small. It is, in fact, smaller in the diffused flow ejector

than in the constant area ejector. This result is consistent with the increased rate of mixing found in the constant area ejector.

At low pressure ratio the surface pressure coefficients are independent of pressure ratio except for the slight increase in the peak suction shown in figure 27. At a pressure ratio of 2.9 the surface pressure coefficient decreases appreciably. In the diffused flow ejector this reduction is primarily due to an improved performance of the diffuser. The pressure recovery in the mixing chamber is similar to that found at other pressure ratios. In the constant area ejector the increased suction is at a pressure ratio of 2.9 in the mixing chamber. These results are in agreement with the expected improvement in mixing associated with the aeroacoustic interaction[34]. Furthermore, the reduced pressure in the mixing chamber undoubtedly is accompanied by an increased entrainment and improved conversion from internal to kinetic energy of the primary flow. The effects of primary flow total temperature on the surface pressure distribution are comparatively small as can be seen in the peak suction values (figure 27). Only at high pressure ratios ($P_o/P_{amb}>2$) is the effect of temperature ratio more pronounced, causing a reduced pressure coefficient as the temperature is increased.

The thrust augmentations at low primary nozzle pressure ratio (<2.5) of the two ejector configurations are 1.21 and 1.32 (∓ 0.05) for the constant area and diffused flow configurations respectively. These results are confirmed by the surface pressure measurements in the high temperature facility. These values are independent of pressure ratio. Only at a pressure ratio of 2.9 does a 10 percent increase in the thrust augmentation ratio occur. There are indications that this may be due to the aeroacoustic interaction[34] as discussed above. The effects of primary nozzle temperature ratio on thrust augmentation are small and within the uncertainty of the measurements.

V. CONCLUSIONS

1. Two characteristic ejector lengths have been identified. They are a minimum length L_m below which flow separation occurs at least on one shroud, and a critical length L_c linked to the evolution of turbulent momentum transport (U'V' velocity profiles) inside the ejector. This critical length L_c characterizes the transition between short and long ejectors as reported by Quinn and Tonis[34]. Conservative estimates of these lengths are $L_m/H=2.5$ and $L_c/H=6.2$.

2. The above characteristic lengths divide the ejector flow field into three distinct regions: the entrance region ($x<L_m$) where the primary jet and shroud surface do not interact directly, the interaction region ($L_m<x<L_c$) characterized by an increase in momentum near the shroud surface, and the "pipe" flow region ($L_c<x$) characterized by an increased skin friction. The first two regions are readily identified in the measured velocity field and surface temperature results. The third region was not present in the configurations investigated because the ejector length was shorter than L_c.

3. Primary jet growth is significantly reduced by the ejector shroud as a result of the coflowing induced flow. The gain in the associated centerline velocity at a fixed downstream location is a function of the pressure ratio and the shroud geometry.

4. The normalized turbulent properties in the ejector are reduced by the coflowing stream as compared to free-jet values. This reduction is of the order of 25 percent.

5. Normalized mean flow profiles and turbulent correlations are not influenced by nozzle pressure ratios up to a value of 2.0.

6. Primary nozzle pressure ratio does not influence the thrust augmentation ratio except at the maximum pressure ratio tested, 2.9, where an

increase of 10 percent was observed. This increased augmentation is believed to result from the aeroacoustic interaction[33]. This mechanism is supported by the observed increase in the noise level inside the facility and by the surface temperature results.

7. Primary nozzle total temperature does not significantly alter the thrust augmentation ratio within the accuracy of the present measurements up to a value of 540°C.

VI. REFERENCES

1. Viets, H. (1975), "Thrust Augmenting Ejectors", ARL 75-0224.

2. Porter, J. L. and Squyers, R. A. (1981), "A Summary/Overview of Ejector Augmentor Theory and Performance", Vols. I, II, Vought Corporation, ATC Report R-91100-9CR-47.

3. Quinn, B. (1981), "Thrust Augmenting Ejectors: A Review of the Application of Jet Mechanics to V/STOL Aircraft Propulsion", AGARD-CPP-308.

4. Green, K. A. and Cyrus, J.D. (1977), "Thrust Augmenting Ejector Technology for Navy Aircraft", AIAA paper 77-1239.

5. Whittley, D. C. and Koenig, D. G. (1980), "Large Scale Model Tests of a New Technology V/STOL Concept", AIAA paper 80-0233.

6. Quinn, B. (1973), "Compact Ejector Thrust Augmentation", J. Aircraft, Vol. 10, pp. 481-486.

7. Bevilaqua, P. M. (1974), "Evaluation of Hypermixing for Thrust Augmenting Ejectors", J. of Aircraft, Vol. 11, pp. 348-354.

8. Sarohia, V., Bernal, L. and Bui, T. (1981), "Entrainment and Thrust Augmentation in Pulsatile Ejector Flows", JPL Publication 81-36.

9. Von Karman, T. (1949), "Theoretical Remarks on Thrust Augmentation", Reissner Anniversary Volume, Contributions to Applied Mechanics.

10. Nagaraja, K. S. (1981), "Some Ejector Characteristics", AIAA paper 81-1679.

11. Nagaraja, K. S., Hammond, D. L. and Graetch, J. E. (1973), "One-Dimensional Compressible Ejector Flows", AIAA paper 73-1184.

12. Alperin, M., and Wu, Jiunn-Jeng. (1983) "Thrust Augmenting Ejectors", AIAA Journal, Vol. 21, No. 10.

13. Hill, P. G. (1965), "Turbulent Jets in Ducted Streams", J. Fluid Mech., Vol. 22, pp. 161-186.

14. Hill, P. G. (1967), "Incompressible Jet Mixing in Converging-Diverging Axisymmetric Ducts", J. of Basic Engineering, March 1967, pp. 210-220.

15. Hickman, K. E., Hill, P. G., and Gilbert, G. B. (1972), "Analysis and Testing of High Entrainment Single-Nozzle Jet Pumps with Variable-Area Mixing Tubes", NASA CR-2067.

16. Bevilaqua, P. M. (1978), "Lifting Surface Theory for Thrust-Augmenting Ejectors", AIAA Journal, Vol. 16, pp. 475-481.

17. Gilbert, G. B., and Hill, P. G. (1973), "Analysis and Testing of Two-Dimensional Slot Nozzle Ejectors with Variable Area Mixing Sections", NASA CR-2251.

18. Mefferd, L. A., and Bevilaqua, P. M. (1978), "Computer-Aided Design Study of Hypermixing Nozzles", NR 78H-91.

19. Chigier, N. A., Ungut, A. and Yule, A. J. (1978), "Particle Size and Velocity Measurement in Flames by Laser Anemometer", 17th International Symposium on Combustion, University of Leeds.

20. Bernal, L. and Sarohia, V. (1984), "An Experimental Investigation of Two-Dimensional Thrust Augmenting Ejectors: Final Report, Part I", JPL Publication 84-50, Part I.

21. Friedlander, S. K. (1977), "Smoke, Dust and Haze. Fundamentals of Aerosol Behavior", John Wiley & Sons, New York.

22. Drain, L. E. (1980), "The Laser Doppler Technique", John Wiley & Sons., London.

23. McLaughlin, D. K., and Tiederman, W. G. (1973), "Biasing Correction for Individual Realization of Laser Anemometer Measurements in Turbulent Flows", "The Physics of Fluids, Vol. 16, pp. 2082-2088.

24. Dimotakis, P. E. (1976), "Single Scattering Particle Laser Doppler Measurements of Turbulence", AGARD CP-193.

25. ASME (1971), "Fluid Meters, their Theory and Application", 6th Edition.

26. Harsha, P. T. (1971), "Free Turbulent Mixing: A Critical Evaluation of Theory and Experiment", AEDC TR-71-36.

27. Van Der Hegge Zijnen, B. G. (1958), "Measurements of the Velocity Distribution in a Plane Turbulent Jet of Air", Appl. Sci. Res. Sec. A., Vol. 7, pp. 256-276.

28. Bradbury, L. J. S. (1965), "The Structure of a Self-Preserving Turbulent Plane Jet", J. Fluid Mech., Vol. 23, pp. 31-64.

29. Gutmark, E. and Wygnanski, I. (1976), "The Planar Turbulent Jet", J. Fluid Mech., Vol. 73, pp. 465-495.

30. Hussain, A. K. M. F. and Clark, A. R. (1977), "Upstream Influence on the Near Field of a Plane Turbulent Jet", The Physics of Fluids, Vol. 20, pp. 1416-1426.

31. Massier, P. F., Back, L. H., Noel, M. B. and Sahelli, F. (1970), "Viscous Effects on the Flow Coefficient for a Supersonic Nozzle", AIAA Journal, Vol. 8, pp. 605-607.

32. Back, L. H. and Cuffel, R. F. (1971), "Turbulent Boundary Layer and Heat Transfer Measurements Along a Convergent-Divergent Nozzle", J. of Heat Transfer, November 1971, pp. 397-407.

33. Quinn, B. (1977), "Interactions Between Screech Tones and Ejector Performance", J. Aircraft, Vol. 15, pp. 467-473.

34. Quinn, B. and Toms, H. L. (1975), "Mixing Duct Pressure Distributions and Exhaust Flow Characteristics of a High Temperature and Pressure Cylindrical Ejector", ARL 75-0227.

35. Bradbury, L. J. S. and Riley, J. (1967), "The Spread of a Turbulent Plane Jet Issuing into a Parallel Moving Airstream", J. Fluid Mech., Vol. 27, pp. 381-394.

NASA—JPL—Coml., L.A., Calif.